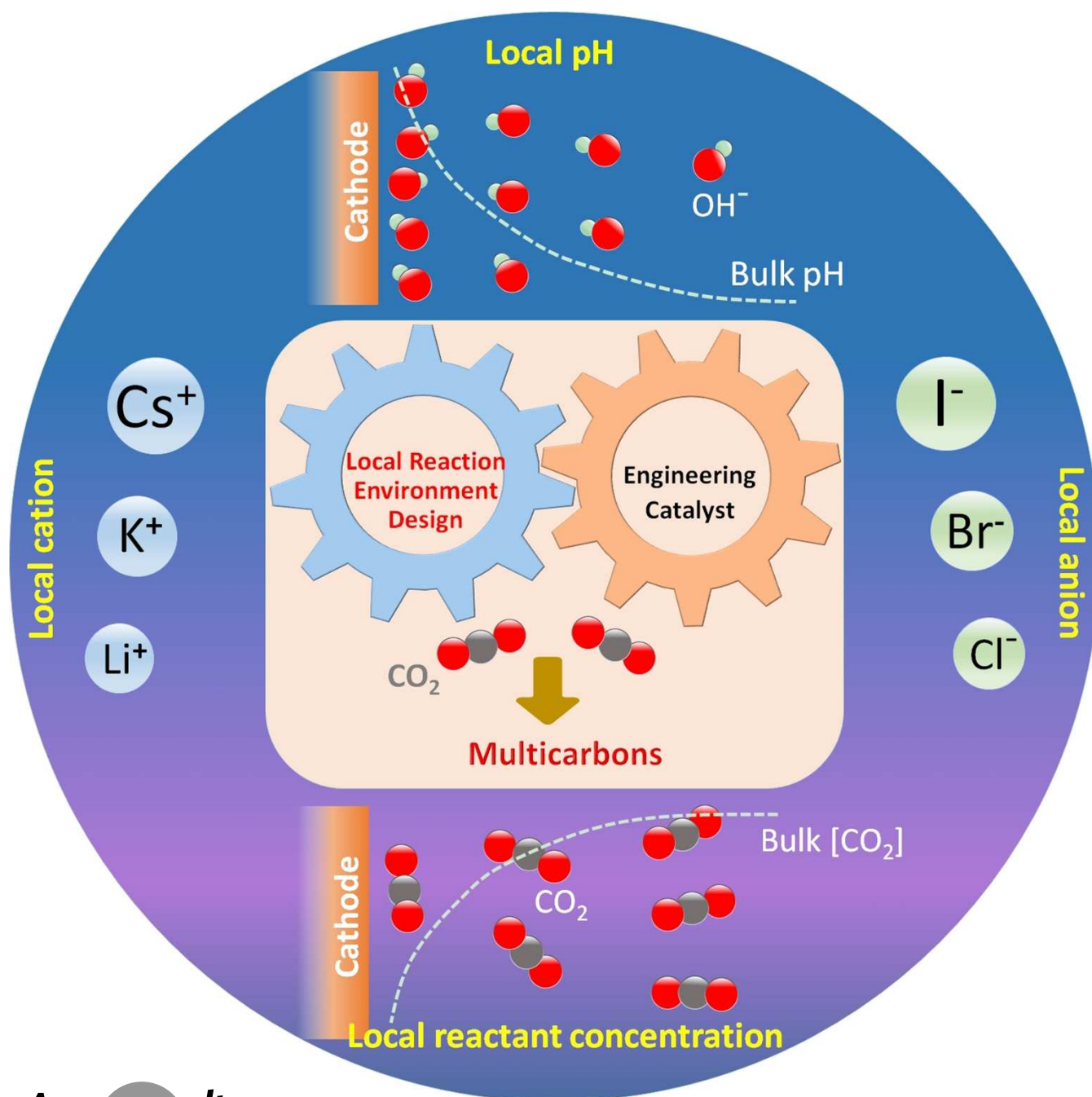


CO₂ Utilization**Rational Design of Local Reaction Environment for Electrocatalytic Conversion of CO₂ into Multicarbon Products**

Ming Ma* and Brian Seger*



Abstract: The electrocatalytic conversion of CO₂ into multi-carbon (C₂₊) products provides an attractive route for storing intermittent renewable electricity as fuels and feedstocks with high energy densities. Although substantial progress has been made in selective electrosynthesis of C₂₊ products via engineering the catalyst, rational design of the local reaction environment in the vicinity of catalyst surface also acts as an effective approach for further enhancing the performance. Here, we discuss recent advances and pertinent challenges in the modulation of local reaction environment, encompassing local pH, the choice of the species and concentrations of cations and anions as well as local reactant/intermediate concentrations, for achieving high C₂₊ selectivity. In addition, mechanistic understanding in the effects of the local reaction environment is also discussed. Particularly, the important progress extracted from in situ and operando spectroscopy techniques provides insights into how local reaction environment affects C–C coupling and key intermediates formation that lead to reaction pathways toward a desired C₂₊ product. The possible future direction in understanding and engineering the local reaction environment is also provided.

1. Introduction

The electrocatalytic conversion of CO₂ into fuels and valuable chemicals powered by renewable electricity not only offers a promising route for the utilization of the captured CO₂ from large emission sources, but also paves the way to the storage of intermittent renewable energy in the form of chemical bonds.^[1–3] In CO₂ electrolysis field, the synthesis of single-carbon products that only involves two-electron transfer, such as CO, has been well developed and is nearing commercial deployment. However, the electrochemical conversion of CO₂ into multicarbon hydrocarbons and oxygenates (C₂₊), such as C₂H₄ and C₂H₅OH, is more attractive owing to their widespread market potential and compatibility with the existing energy infrastructures.

To date, the most promising catalyst is still Cu, which can electrochemically catalyze the production of C₂₊ with appreciable selectivity at high reaction rates under mild conditions.^[4–6] Over the past decades, great efforts have been expended to develop selective and efficient Cu-based electrocatalysts by tuning the morphologies,^[7,8] crystal facets,^[9,10] oxidation states^[11,12] and compositions of the catalysts.^[13,14] For instance, the best ethanol selectivity reported so far is ~52 % with a partial current density of ~150 mA/cm² by coating Cu with nitrogen-doped carbon.^[15] After considering CO₂ consumption (e.g. measuring outlet gas flowrate) at gas diffusion electrodes (GDEs) and the

corresponding issue of CO₂ utilization rate at high-rate electrolysis,^[16] recently reported C₂H₄ selectivity is no more than 50 % in acidic CO₂ electrolysis.^[17–20] Although significant progress has been made on the improvement of selectivity and activity for CO₂ reduction (CO₂R) to C₂₊ products, the performance toward a desired C₂₊ product through solely engineering the catalyst still cannot achieve the metrics required for practical utilization of CO₂ electrolysis technology.^[2,21]

The electrosynthesis of C₂₊ products from CO₂ occurs in the electrolyte, and the formation of numerous intermediates in multistep reaction process toward C₂₊ products involves the complex interaction between an electrode and the reaction environment at the electrode/electrolyte interface. The local reaction environment in the vicinity of catalyst surface, such as local pH, ionic species and concentrations as well as local reactant/intermediates concentrations, has a significant effect on the formation and coverage of intermediates in CO₂R.^[3,22] The coverage of key intermediates on catalyst surface is closely correlated with reaction pathways toward specific C₂₊ products, determining final product formation. Thereby, rationally controlling the local reaction environment has attracted significant interest as an alternatively promising strategy for further improving the selectivity and activity toward a desired C₂₊ product at relatively low overpotentials.

This review aims at discussing some recent advances and outstanding challenges in the modification of local reaction environment for tuning the catalytic selectivity and activity in electrocatalytic CO₂ conversion. Specifically, we mainly focus on the important progress in the effects of local pH, the choice of electrolyte (the species and concentrations of cation and anion) and local reactant/intermediate concentrations (Figure 1). Additionally, the efforts from in situ and operando spectroscopy methods are also discussed, followed with mechanistic insights into the role of the local reaction environment in C–C coupling, intermediates formation and related reaction pathways toward a desired C₂₊ product.

2. Local pH Effects

In CO₂R, one of the most significant parameters is the pH that is associated with the formation of certain intermediates, and the coverage of intermediates could influence the

[*] Dr. M. Ma
School of Chemical Engineering and Technology
Xi'an Jiaotong University
Xi'an 710049, People's Republic of China
E-mail: mingma@xjtu.edu.cn
Prof. B. Seger
Surface Physics and Catalysis (Surfcat) Section
Department of Physics
Technical University of Denmark
2800 Kgs. Lyngby, Denmark
E-mail: brse@fysik.dtu.dk

© 2024 The Authors. Angewandte Chemie published by Wiley-VCH GmbH by Wiley-VCH GmbH. This is an open access article under the terms of the Creative Commons Attribution Non-Commercial NoDerivs License, which permits use and distribution in any medium, provided the original work is properly cited, the use is non-commercial and no modifications or adaptations are made.

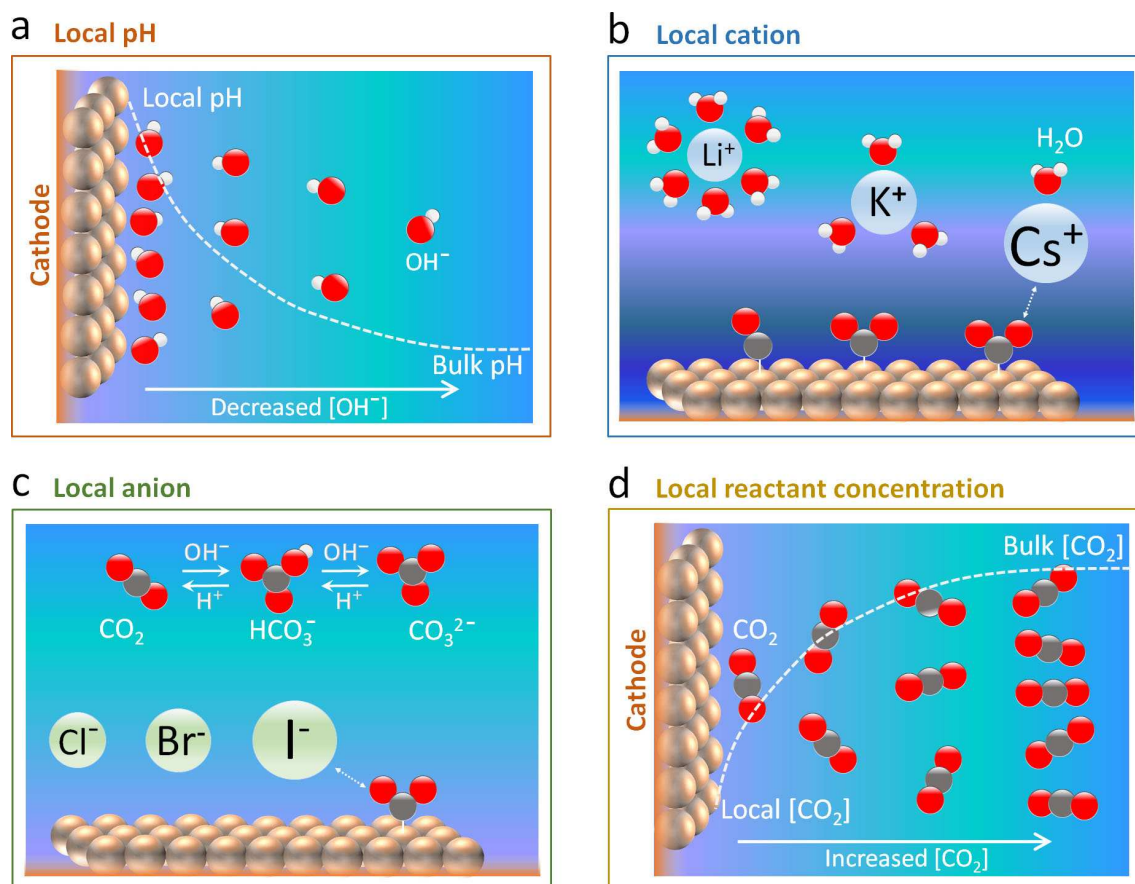
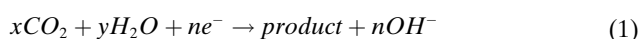


Figure 1. Overview of local reaction environment effects in CO_2 reduction discussed in this review. a), Local pH effects. b), Cation effects. c), Anion effects. d), Local reactant concentration effects. The red, white and grey balls represent O, H and C atoms, respectively.

reaction pathways that determine the final products. The pH rises locally at the cathode/electrolyte interface owing to the OH^- production in the CO_2R and H_2 evolution reaction (HER), and the OH^- production rate is linearly correlated with current densities according to the reactions below:



The effect of local pH near the Cu cathode was initially proposed by Hori et al.,^[23,24] revealing the correlation of the local pH with catalytic selectivity and activity of C_2H_4 and

CH_4 in a H-cell reactor. In this section, we review the recent advances in the modulation of local pH for selective CO_2R as well as the related mechanistic insights via CO electrolysis and local pH determination methods. We also discuss low carbon utilization triggered by local alkaline environment at high-rate CO_2 electrolysis.



Ming Ma obtained his PhD at Department of Chemical Engineering, Delft University of Technology in 2017. After that, he worked as a postdoc at Delft University of Technology. In 2018, he moved to Denmark, working as a postdoc at Department of Physics, Technical University of Denmark. Since 2021, he has been an associate professor at School of Chemical Engineering and Technology, Xi'an Jiaotong University. His research interest mainly focuses on the electrochemical conversion of CO_2 .



Brian Seger has been a full Professor in DTU Physics since 2022. He did his PhD at the University of Notre Dame followed by a post-doc at the University of Queensland, before moving to DTU in 2011. His earlier work focused on photoelectrocatalytic water splitting, most notably on protection layers. In the last 5 years his research shifted towards electrosynthesis with a focus on CO_2 electrolysis. Throughout his career he has published 80 works in these fields.

2.1. Tuning Selectivity

The different buffering strengths of the electrolytes can influence the amount of neutralization reaction for OH^- ions generated via cathodic reactions, correspondingly tailoring the local pH near the catalyst surface. For instance, 0.1 M K_2HPO_4 can easily neutralize OH^- near the surface of cathode, keeping local pH at relatively low value that corresponds to the high selectivity of H_2 and CH_4 along with suppressed C_2H_4 formation (as shown in Table 1).^[23] In contrast, 0.1 M KClO_4 or K_2SO_4 does not have buffer ability, resulting in a relatively high local pH that offers a high C_2H_4 selectivity. Thereby, early examples used electrolytes with different buffer capacities (such as KClO_4 , K_2SO_4 , KHCO_3 and K_2HPO_4) to explore the local pH effect on product distribution over Cu surface during CO_2R in traditional H-cell reactors, finding that a locally high pH region created near the electrode suppresses the formation of CH_4 and H_2 , correspondingly favoring selectivity of C_2H_4 .^[7,23–26]

In addition, the cathodic morphology also can influence the local pH. A highly nanostructured surface not only provides the large electrochemical active surface area needed for high current densities (i.e. enhanced OH^- production rate), but also has the function of confining locally generated OH^- due to limited diffusion process within the nano-morphology. Thus, a highly nanostructured surface is able to modify the local pH, which is widely accepted as one of the possibilities that tune catalytic selectivity in CO_2R when using nanostructured catalysts.^[3,7,12,27–29] For instance, it was reported that systematically varying the length and density of the Cu nanowires can provide a high local pH within the nanowire arrays via the confined diffusion of generated OH^- , thus tailoring the selectivity of hydrocarbon products (such as C_2H_4 , a gradual increase in selectivity from ~2% to ~17%) on Cu nanowire arrays.^[7] Additionally, high surface roughness^[27] or high-curvature surfaces^[12] of nanostructure could induce high current densities (i.e. enhanced OH^- production rate), leading to high local pH. The relatively high local pH restricts the HER^[7] and the protonation of bound CO intermediate that leads to the formation of CH_4 ,^[12] contributing to an enhanced C–C coupling toward C_{2+} production.

For understanding the local pH effect, rotating ring-disk electrode technique was applied,^[30–34] owing to that this technique provides an effective method for the modulation of local pH gradient through varying the mass transport of anion species (such as OH^-) that is linked to the rotation

speeds. Specifically, with increasing the rotation (mass transport) speeds, the locally generated hydroxyl ions are transported away from the electrode surface at an accelerated rate,^[35] decreasing the local alkalinity. By comparing the catalytic performance of a polycrystalline Cu disk cathode with different rotation speeds, it was discovered that the electrocatalytic CO_2R was suppressed upon increasing the rotation speeds, accompanying with an enhanced hydrogen evolution reaction.^[30] This finding may be linked to a decrease in the alkalinity near the Cu surface with an increase in the rotation speed. However, the increased rotation speed also influences the local reactant concentrations via enhanced convection, namely, increased local CO_2 concentration and decreased local intermediate concentrations (such as CO). Thus, variations in the local reactant/intermediate concentration may be also partially responsible for the catalytic performance observed on rotating Cu-disk when considering local pH effect.

Recently, coating the cathode with ion-conducting ionomer has been shown to enable a tunable local pH via the control of ion transport on the cathode, resulting in a variation in CO_2 reduction products.^[36–38] For instance, covering Cu with Nafion (a cation-conducting film) can lead to a significantly enhanced C_{2+} selectivity with inhibited H_2 evolution, since Donnan exclusion induced by the negative background charge in Nafion enables an accumulation of OH^- generated via cathodic reactions on the Cu surface (i.e. enhanced local pH).^[37,39] Subsequently, the bilayer of Sustainion (an anion-conducting film) covered with Nafion not only promotes a high local pH but also tunes local $\text{CO}_2/\text{H}_2\text{O}$ ratio near the surface of Cu, thereby resulting in 90% selectivity for C_{2+} formation with only 4% H_2 selectivity at 12 mA/cm^2 (–1.15 V vs. reversible hydrogen electrode).^[37]

All the above examples in traditional H-cell reactors reveal that C_{2+} selectivity in CO_2 electrolysis can be tuned by tailoring the local pH via buffer capability of the bulk electrolyte (Figure 2a) and mass transport of ionic species (Figure 2b) near the Cu surface. The mass transport of ionic species near the cathode can be influenced by surface morphology, rotating ring-disk electrode technique and ionomer coating (Figure 2b). In addition, while high local pH can improve catalytic selectivity in CO_2R , the local CO_2 concentration may decrease via neutralization reaction in local alkaline environment (particularly in H-cells), thereby attention should also be paid to the balance between high local pH and local reactant concentration.

2.2. Mechanistic Exploration via CO Reduction

CO_2 forms carbonate or bicarbonate via buffering reaction in alkaline electrolytes, which leads to significant changes in ionic species and pH of electrolyte.^[16] While CO can react with OH^- to produce formate, the reaction rate is extremely slow, thus having negligible influence on ionic species and pH of alkaline electrolyte.^[40] Additionally, CO serves as the key intermediate for C–C coupling that leads to the formation of C_{2+} products. Thereby, in order to gain mechanistic insights into the effect of local pH on the

Table 1: Faradaic efficiencies for major products in CO_2 -saturated 0.1 M various solutions over Cu foil at 5 mA/cm^2 in a H-cell reactor. Table was adapted from Ref. [23].

Solution	pH	Faradaic efficiency (%)					
		CH_4	C_2H_4	Ethanol	CO	Formate	H_2
KClO_4	5.9	10.2	48.1	15.5	2.4	8.9	6.7
K_2SO_4	5.8	12.3	46.0	18.2	2.1	8.1	8.7
KHCO_3	6.8	29.4	30.1	6.9	2.0	9.7	10.9
K_2HPO_4	6.5	17.0	1.8	0.7	1.3	5.3	72.4

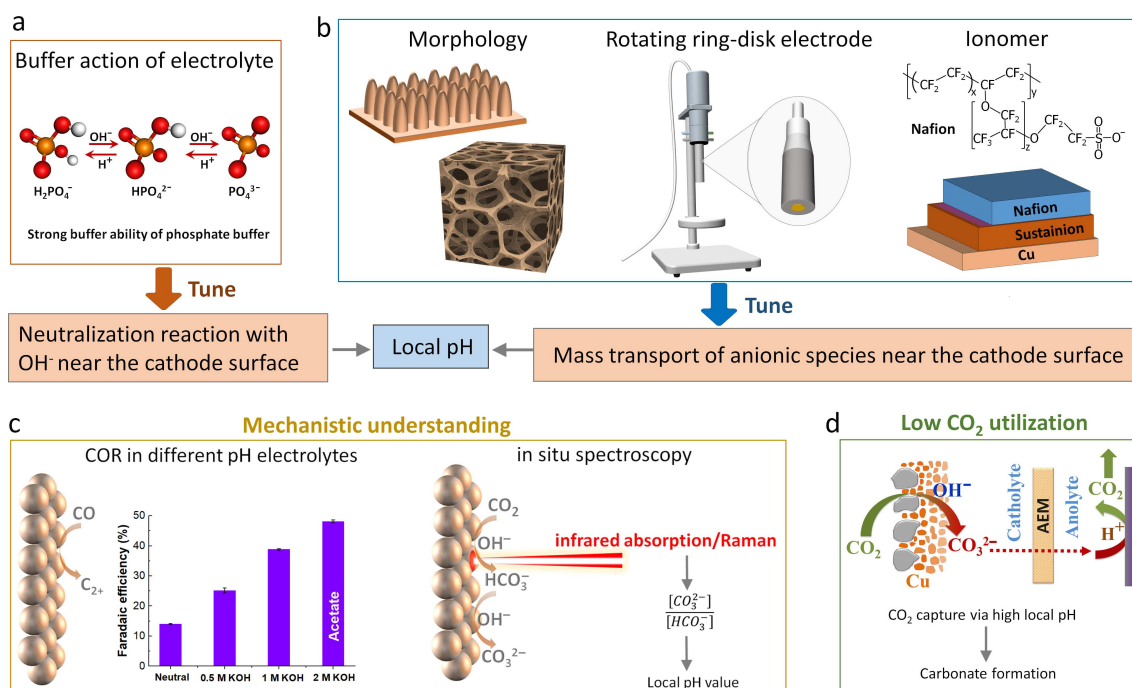
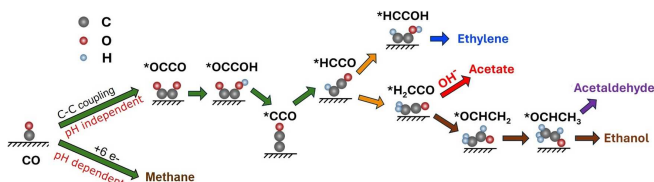


Figure 2. Local pH effects in CO_2 reduction. **a**), Buffer action of electrolyte for neutralizing local pH. **b**), Mass transport of ionic species for tuning local pH. **c**), Mechanistic exploration via CO reduction (left, data of acetate selectivity in different pH electrolyte is from Ref. [40]) and local pH determination (right). **d**), Low carbon utilization triggered by local alkaline environment.

formation of CO_2 reduction products and to achieve tunable selectivity toward a desired C_{2+} , CO electrolysis has been explored in distinct pH electrolytes (Figure 2c, left).

The pioneering work performed in H-cells has demonstrated the correlation of pH with the specific products formation in CO reduction (COR) on Cu surface.^[41–43] The analysis of activity versus overpotential reveals that while the formation rate of CH_4 involves proton transfer and is pH-dependent (Scheme 1), the formation rates of C_2H_4 and $\text{C}_2\text{H}_5\text{OH}$ are independent of pH, thus leading to the observed variation in selectivity ratio of C_{2+}/C_1 in different pH solutions.^[43] A comparison of the product distributions between COR and CO_2R also suggests that the rate-determining step for C_{2+} formation is pH-independent on the SHE scale.^[44]

In addition, in the most accepted theory, the CO dimerization is the key reaction step toward C_{2+} products



Scheme 1. Possible reaction paths for CO reduction, with path (i), showing pH-dependent CH_4 formation (high local pH inhibits CH_4 formation), and path (ii), showing pH-independent C–C coupling. Reaction Scheme adapted from developments derived in Ref. [40,44,49,54] with the Figure being a modified version of Ref. [55].

on Cu surface, and CO dimer that does not involve the proton transfer should be pH-independent,^[45–48] which reflects the key step of C_{2+} formation irrespective of pH, as shown in Scheme 1. Furthermore, a combination of electrokinetic and in situ spectroscopic studies in CO reduction on Cu also indicates distinct pH-dependent behaviors in formation rates of CH_4 and C_{2+} products that are likely limited by the dimerization of CO.^[49] While all the aforementioned studies performed in traditional H-cells provide significant understanding of the role of (local) pH in CO electrolysis, the exceedingly low CO solubility in solutions dramatically restricts CO mass transport to the surface of the cathode, which may affect the mechanistic insights on pH effect in CO reduction. In order to eliminate the effect of mass transport limitations and to unveil a more accurate correlation of the local pH with the catalytic selectivity, recent work of CO electrolysis in distinct pH electrolytes has been performed in flow-electrolyzers with gas diffusion electrodes,^[40,50,51] which can significantly accelerate the mass-transport of reactant (i.e. CO) and gaseous products.^[52,53] Using GDE-type flow electrolyzers, the Jiao group discovered an increased production ratio of acetate to other C_{2+} products in alkaline electrolyte at high-rate CO reduction.^[50] A combination of transport calculations and isotopic labeling suggests that a higher local pH facilitates the production of acetate via the possible reaction of OH^- with a certain intermediate.^[50] This finding is consistent with the previous work in H-cell that also showed more favorable production of acetate from CO reduction in alkaline conditions.^[44]

To provide the direct evidence of the link between local pH and specific C_{2+} selectivity, we recently developed a

very simple strategy for experimentally determining the local pH in GDE-based high-rate CO electrolysis, thus we explicitly demonstrated a gradually enhanced acetate selectivity from 14 % to nearly 50 % upon systematically increasing OH⁻ concentration in the vicinity of cathodic GDE surface (Figure 2c, left), concomitantly inhibiting other C₂₊ formation such as C₂H₄ (selectivity decreased from ~45 % to ~34 %) and ethanol (selectivity decreased from ~15 % to ~5 %).^[40] It should be noted that although specific C₂₊ selectivity is locally pH-dependent, we found that the total C₂₊ formation is almost pH-independent in alkaline conditions (nearly identical Faradaic efficiency of ~90 % for total C₂₊ in various KOH concentrations).^[40]

Regarding the formation mechanism of acetate influenced by OH⁻ in CO electrolysis, the rate determining step for acetate may be different from the other C₂₊ products,^[44] and it was reported by Birdja and Koper^[56] that acetate may be (partially) formed from Cannizzaro-type disproportionation of acetaldehyde promoted by local alkaline environment. Although the ethanol formation seems to be always accompanied with acetate, the molar ratios of ethanol to acetate produced in COR work were far from equal,^[40] which indicates that the majority of acetate may be formed via a distinct reaction pathway rather than disproportionation of acetaldehyde. It has been shown that OH⁻ can react with ketene to form acetate in solutions,^[57,58] and recent simulation work based on density functional theory (DFT) has also demonstrated that the electrosynthesis of acetate from CO is likely through ketene intermediate that is catalyzed by OH⁻.^[59] Notably, this key step for acetate formation is a homogeneous solution reaction that is directly influenced by local pH near the cathode instead of bulk pH.^[40] Additionally, acetaldehyde oxidation induced by OH⁻ may also partially contribute to acetate formation.^[55]

Additionally, Jouny et al. provided further evidence of the ketene intermediate by adding amines (such as methylamine and dimethylamine) in the solvent during CO electrolysis, producing various amides.^[60] The production of amides was explained by a nucleophilic attack on the ketene (i.e. ethenone) by the amines. Since the amine competes with OH⁻ to react with the ketene intermediate, the amides replaced the selectivity for ethanol/acetate but not for ethylene, which further validates the area where the branching occurred. Recently, the Kastlunger group showed adding microkinetic models to account for reaction kinetic barriers for DFT-calculated thermodynamic values of intermediates,^[54] which denotes some of the past limitations of previous approaches and how this could result in misleading hypotheses of mechanisms.

2.3. Local pH Determination

Quantifying the local pH value during electrolysis is highly desirable to gain a better understanding of the catalytic performance. CO₂ not only works as a reactant but also acts as a buffer (neutralization with OH⁻), thus making the local reaction environment complicated (uncertainty of local pH and reactant concentration).^[61] Gupta et al. developed an

initial mathematical model with the consideration of the CO₂ consumption, relevant diffusion process, and current-induced OH⁻, theoretically showing a pH profile near the Cu surface in CO₂R.^[62] Theoretical calculations showed an enhanced local pH value at elevated current densities.^[25,52,63] For instance, the pH value increased from ~10 at 1 mA/cm² to more than 12 at 100 mA/cm² under identical conditions.^[63]

Experimentally, in situ spectroscopy techniques have been commonly employed to probe the local pH during CO₂R via comparing relative integration of pH-sensitive electrolyte species signals near the surface of the electrode (Figure 2c, right).^[64–69] For instance, the pH near the cathode during CO₂R can be determined by the relative integration of CO₃²⁻ and HCO₃⁻ signals, provided by in situ surface-enhanced infrared absorption spectroscopy (SEIRAS) in the attenuated total reflection (ATR) mode.^[64] SEIRAS can also offer the comparison of phosphate buffer species near cathode surface to estimate the local pH value.^[65] Particularly, for determining the local pH near the cathodic GDE at commercially current densities, in situ Raman spectroscopy has been reported to be a powerful tool.^[67,68] Although spectroscopy techniques enable to probe local pH, they are limited to only special systems with pH-sensitive electrolyte species signals. Recently, a fluorescent confocal laser scanning microscopy (CLSM) was employed to create maps of the local OH⁻ concentration near a copper-coated GDE.^[63] The CLSM can map pH in 3D, but a fluorescent added into the electrolyte may affect electrolysis. In addition, rotating ring-disk electrode technique^[70] and scanning electrochemical microscopy pH sensor^[71] were also shown to be capable of determining the local pH in CO₂R, whereas whether these methods are applicable to high-rate CO₂R is unclear. Furthermore, we reported a simple local pH determination method in high-rate CO reduction on the basis of CO₂ capture rate via reaction with OH⁻.^[40]

All of these localized pH probe techniques demonstrated an increase in local pH at elevated current densities. However, in GDE-based high-rate CO₂R, we did not observe apparent variations in C₂₊ selectivity upon increasing current densities,^[16] which may be attributed to that current-induced OH⁻ near the cathodic GDE/electrolyte interface is significantly neutralized by CO₂ that is supplied sufficiently and rapidly through GDEs.

Additionally, high local pH detected near the cathode surface during electrolysis, especially at elevated current densities, indicates very low H⁺ concentration near the cathode. Considering that high-rate COR is widely performed in alkaline electrolytes, local H⁺ source near the cathode is dramatically limited, thereby the proton donor in CO₂R/COR should derive from water instead of H⁺. This statement agrees with recent discoveries in mildly acidic media.^[72–74] In most of the cases (with the exception of using acidic electrolytes), the dominant proton donor for the competing HER also stems from water.^[31,52,72] Even in mild acid, proton reduction to H₂ can be significantly suppressed through neutralizing H⁺ with OH⁻ generated in CO₂R.^[75]

2.4. Low CO₂ Utilization at High Current Densities

In the past, highly concentrated KOH electrolytes (i.e. high alkalinity environment) was commonly employed in GDE-type flow electrolyzers for increasing the electrolyte conductivity and reducing the overpotentials for high-rate CO₂R.^[1,2,76] However, a substantial amount of CO₂ reactant is captured at the cathodic GDE/electrolyte interface via reaction with OH⁻, forming CO₃²⁻, as shown in Figure 2d.^[16,77] Even in relatively neutral electrolytes, we found that ~70% of the total consumed CO₂ was captured in the form of CO₃²⁻ via high local pH created near cathodic GDE, which not only influences the quantification of gas products (due to gas flow variation) but also leads to low carbon utilization (only ~30%).^[16]

Many attempts have been made in order to minimize loss of CO₂ feedstock induced by carbonate formation and to increase the utilization of CO₂ input at high-rate CO₂ electrolysis.^[78] Here, we classified all these attempts into two main strategies: (i) regeneration of CO₂ from carbonate and subsequent reuse in CO₂ reduction as well as (ii) a cascade approach with CO₂R to CO and subsequent COR to C₂₊. Specifically, carbonate formation (i.e. CO₂ capture) near the cathodic GDE is inevitable owing to high local OH⁻ concentration created via cathodic reactions in GDE-type flow electrolyzers.^[16,77-79] Thus, for enhancing carbon source utilization, regeneration of high-purity CO₂ from the formed carbonate and subsequent recycling has been shown by using bipolar membrane^[80,81] or adding a porous and ion-conducting solid electrolyte buffer layer.^[82] Recently, CO₂R to C₂₊ in acid has been demonstrated to improve the carbon utilization as the formed carbonate can be locally converted back into CO₂ again via neutralization reaction with H⁺ in acid and utilized in situ near the cathode for CO₂R.^[17-19,83] Although acidic CO₂ reduction can significantly enhance carbon utilization, CO₂R does not take place efficiently and selectively owing to kinetically favored HER in acid conditions. To suppress HER in acidic CO₂ reduction, a locally alkaline or neutral environment near the catalyst surface should be created by balancing bulk solution pH and current density.^[18]

In addition, the group of Jiao has proposed a two-step cascade reaction strategy, where CO₂ is initially converted into CO, followed by CO reduction to C₂₊.^[50,77] Subsequently, this cascade strategy has been demonstrated experimentally to improve carbon source utilization.^[84] Although all these emerging strategies can dramatically enhance carbon utilization, how to enhance the commercially relevant long-term stability for the overall system while maintaining high C₂₊ selectivity and minimizing the cell voltage in this process remains a challenge.

2.5. Reactor Configurations

The above-mentioned local pH studies including the pH test and mechanistic explorations were all based on traditional H-cell reactors and GDE-based flowing-catholyte reactors (Figure 3a, left). The two types of reactors contain a

catholyte layer between a cathode catalyst and a membrane. This catholyte layer provides a platform for relatively readily identifying and controlling the local pH discussed in this section and cation/anion species near the cathode in the following sections. Additionally, the catholyte layer also can reduce the effect of the environment near the membrane on the catalytic performance. Typically, the different ion-selective membranes have a negligible effect on catalytic selectivity in GDE-based flowing-catholyte reactors (Figure 3a, right), which is due to that the introduction of the catholyte layer helps to create the similar local pH at the catholyte/electrolyte interface regardless of membrane types under identical conditions.^[80] However, this catholyte layer means the large ohmic resistance that increases the voltage of the whole reactor, which reduces the energy efficiency, restricting the commercialization of this technology.

In a membrane electrode assembly (MEA) electrolyser, a membrane is sandwiched between a cathode catalyst and an anode catalyst (as displayed in Figure 3b, left). This direct contact between catalyst layer and membrane is also referred to as a zero-gap electrolyzer, which can lower the ohmic resistance of the whole reactor, resulting in enhanced energy efficiencies. However, in the MEA configuration, the local environment on the surface of the membrane could significantly affect the catalytic performance due to the direct contact between the catalyst layer and membrane. For instance, when using a cation exchange membrane (Figure 3b, right), the proton generated via anodic reactions (water oxidation) serves as the dominant charge-carrying species, transporting from anode side to cathode side via the cation exchange membrane (CEM), which leads to significantly reduced local pH near the cathodic catalyst. Due to the acidic environment with H⁺ favoring the H₂ formation, the use of the CEM showed unfavorable CO₂ reduction with dominant H₂ evolution in the MEA configuration.^[85] In practice, an anion exchange membrane (AEM) is widely used in MEA design due to that the AEM provides an alkaline environment for the cathode layer via transferring anionic species (such as OH⁻, and carbonate) through the membrane (as shown in Figure 3b, right), and CO₂ conversion is more selective and efficient when occurring in locally neutral to basic pH conditions. Additionally, it should be noted that both GDE-based flowing-catholyte and MEA reactors suffer from low carbon utilization due to inevitable (bi)carbonate formation near cathodic GDE during CO₂ electrolysis, which remains an ongoing challenge for the field.

Considering their unique advantages of the two typical electrolyzers (Figure 3), the effect of reactor configurations on local cation, anion and reactant near the cathode is also taken into account in the following sections.

3. Cation Effects

The nature of electrolyte cations plays an important role in the electrocatalytic selectivity and activity of CO₂R.^[17,72,86] On Cu surfaces, the selectivity toward C₂₊ formation can be steered by varying the size of the alkali metal cations in the

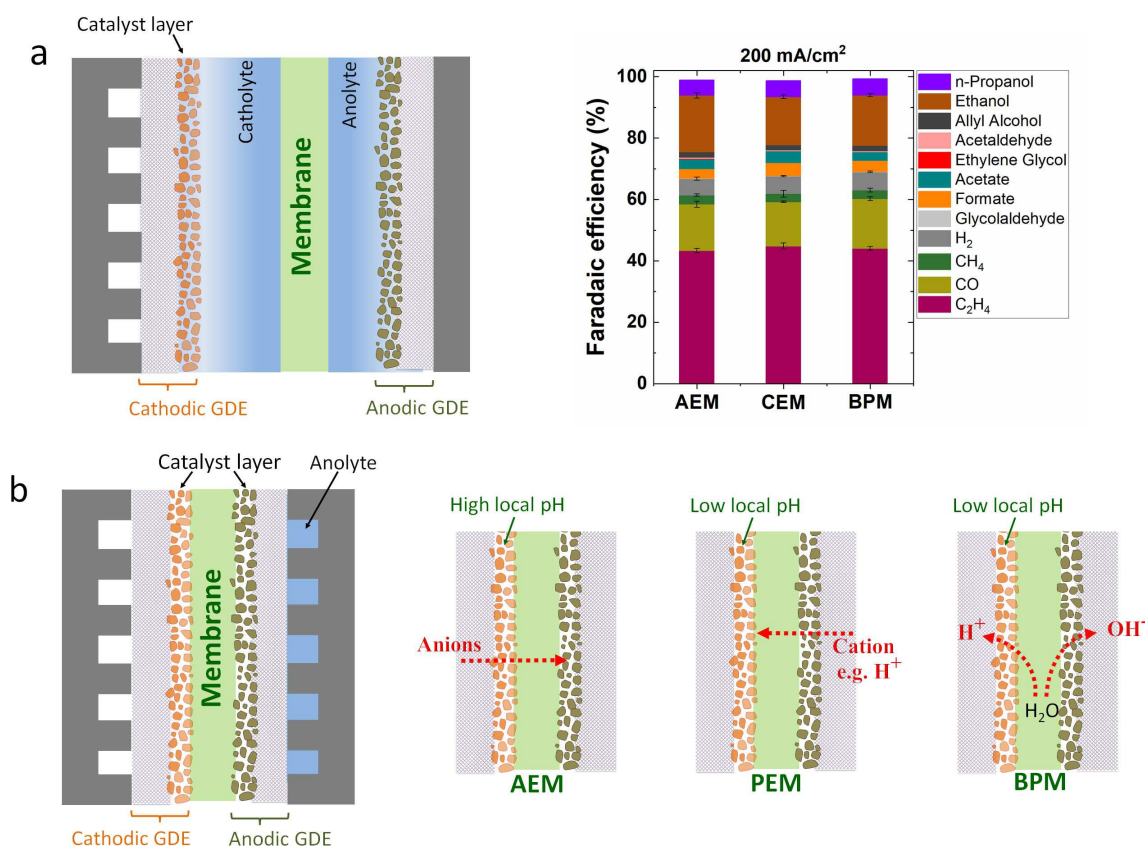


Figure 3. Schematic of reactor configurations for high-rate CO₂ reduction. a), GDE-based flowing-catholyte reactors (left) and membrane effect on catalytic selectivity (right, Figure adapted from permission).^[80] b), Membrane electrode assembly electrolyzers (left) and the charge-carrying ionic species for the different ion-selective membranes (right).

electrolyte. In particular, the dramatically enhanced C₂₊ products such as alcohol and C₂H₄ have been shown with increasing the cation size (in the order of Li⁺ < Na⁺ < K⁺ < Cs⁺) in electrolytes, as presented in Figure 4a.^[87] In contrast, in Li⁺-containing solution (smaller cation size), H₂ evolution was obviously favorable over CO₂ reduction. While the consistent catalytic trends and phenomena were manifested in many different studies regarding cation effects, numerous theories have been proposed to elucidate the cation effects, and the exact mechanistic effect remains controversial. In this section, we divided the previous theories into two main categories: (i) cation-induced pH variation and (ii) interaction with intermediates.

3.1. Tuning pH

The effect of cation on CO₂ reduction selectivity was initially demonstrated on Cu catalysts by Hori and co-workers,^[42] followed with the explanation of the variation of the potentials (E₂) at the outer Helmholtz plane (OHP) caused by the cation species (Figure 4b). In this theory, the value of E₂ is more positive with increasing the cation size in the order of Li⁺ < Na⁺ < K⁺ < Cs⁺, and the more positive E₂ corresponds to a higher local pH at the electrode surface. As discussed in the previous section, the enhanced local pH

inhibits formation of HER and CH₄ while promoting C₂H₄ production at larger cation size.

In contrast to the local electric field effect on pH, another theory attributes product distribution with different cation sizes to the enhanced buffer capability of larger alkali metal cations.^[87] In this hypothesis, the hydrated cations serve as buffering agents to vary the local pH near the cathode, influencing local CO₂ concentration. Specifically, the pK_a for cation hydrolysis reduces with increasing cation size, thus larger cation size could lead to an increase in local concentration of CO₂ by maintaining the local pH at a relatively low value (Figure 4c). Subsequently, in situ SEIRAS^[64] and rotating ring-disk electrode^[70] were employed to determine the local pH with different alkali metal cations during CO₂R, showing that the local pH follows the tendency of Li⁺ > Na⁺ > K⁺ > Cs⁺, which is consistent with the hypothesis of cation hydrolysis.

However, contradictory to the hypothesis of cation hydrolysis (Figure 4c), the Xu group^[88] probed the trend of interfacial CO₂ concentration in situ using SEIRAS in ATR mode, discovering a decrease in local CO₂ concentration with increasing size of alkali metal cations. In addition, the local pH trend with different alkali cations proposed in the hypothesis of cation hydrolysis^[87] contradicts that in the theory of local electric field.^[42] Notably, local CO concentration is not affected by pH, but the hypothesis of cation

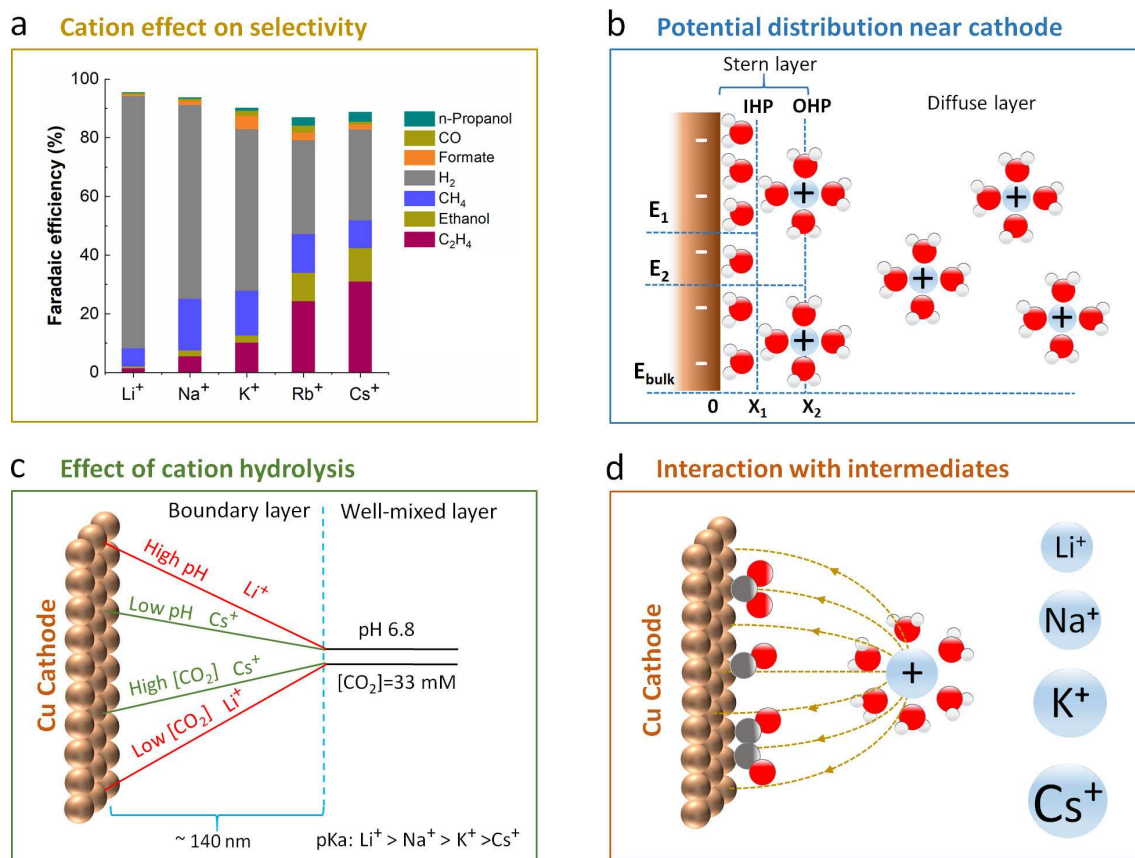


Figure 4. Cation effects in CO₂ reduction. a), Cation effect on catalytic selectivity of CO₂ reduction (Data reproduced from Ref. [87]). b), Potential distribution near cathode. Figure adapted from Ref. [42]. c), Effect of cation hydrolysis. Figure adapted from Ref. [87]. d), Interaction with intermediates. The red, white and grey balls represent O, H and C atoms, respectively.

hydrolysis is unable to explain the similar catalytic trend in COR with increasing cation size.^[42] Future studies require more advanced in situ and operando spectroscopy techniques to further clarify these hypotheses.

3.2. Stabilization of Certain Intermediates

In addition to cation-induced pH variations near the cathode surface, the presence of specifically adsorbed alkali cations on Cu surfaces have been hypothesized to affect the binding strength or coverage of the certain intermediates (Figure 4d).^[89,90] For instance, adsorbed K⁺ may stabilize *CO and *CHO, which makes paths toward C₂₊ products more favorable.^[89] DFT simulation studies suggested that cation-induced stabilization of intermediates was primarily due to local electrostatic interaction between solvated cations at OHP and adsorbed species that possess large dipoles/polarizabilities.^[91–93] In this theory, weakly hydrated cations (i.e. larger cations) experience a stronger driving force of cations toward OHP from bulk solution.^[92] The electric field induced by local cations can stabilize the intermediates,^[91] thus the enhanced activity of C–C coupling toward C₂₊ formation in the presence of larger cations (i.e. weakly

hydrated cations) arises from a higher concentration of the cations accumulated at OHP with increasing cation size.^[92]

To experimentally confirm the correlation of the cation concentration on the cathode surface with catalytic performance, SEIRAS was utilized to probe the displacement of specifically adsorbed tetramethylammonium (methyl₄N⁺) with alkali metal cations.^[94] It was demonstrated that the coverage of alkali metal cations follows the order Li⁺ < Na⁺ < K⁺ < Cs⁺. The authors proposed that the surface coverage of different alkali metal cations is correlated with their free energy of hydration and determines their distinct catalytic performance.^[94]

The role of alkali cation species in CO₂ electrolysis was further explored with and without alkali cations in acidic electrolytes, revealing that CO₂R does not take place without cations, and only adding cations in electrolytes could transform the selectivity from HER to CO₂R.^[17,72] Cations act as the main promoter for enabling CO₂R to occur via stabilizing the key intermediates formation in the pathways toward CO and C₂₊ products.^[72,95–97] In addition, it was proposed that alkali cations accumulated at OHP shield the local electric field, which suppresses HER by decreasing the force for migration of hydronium towards the cathode surface in acidic electrolytes while stabilizing key intermediates in CO₂R (Figure 5a).^[74] Thus, cation has been widely

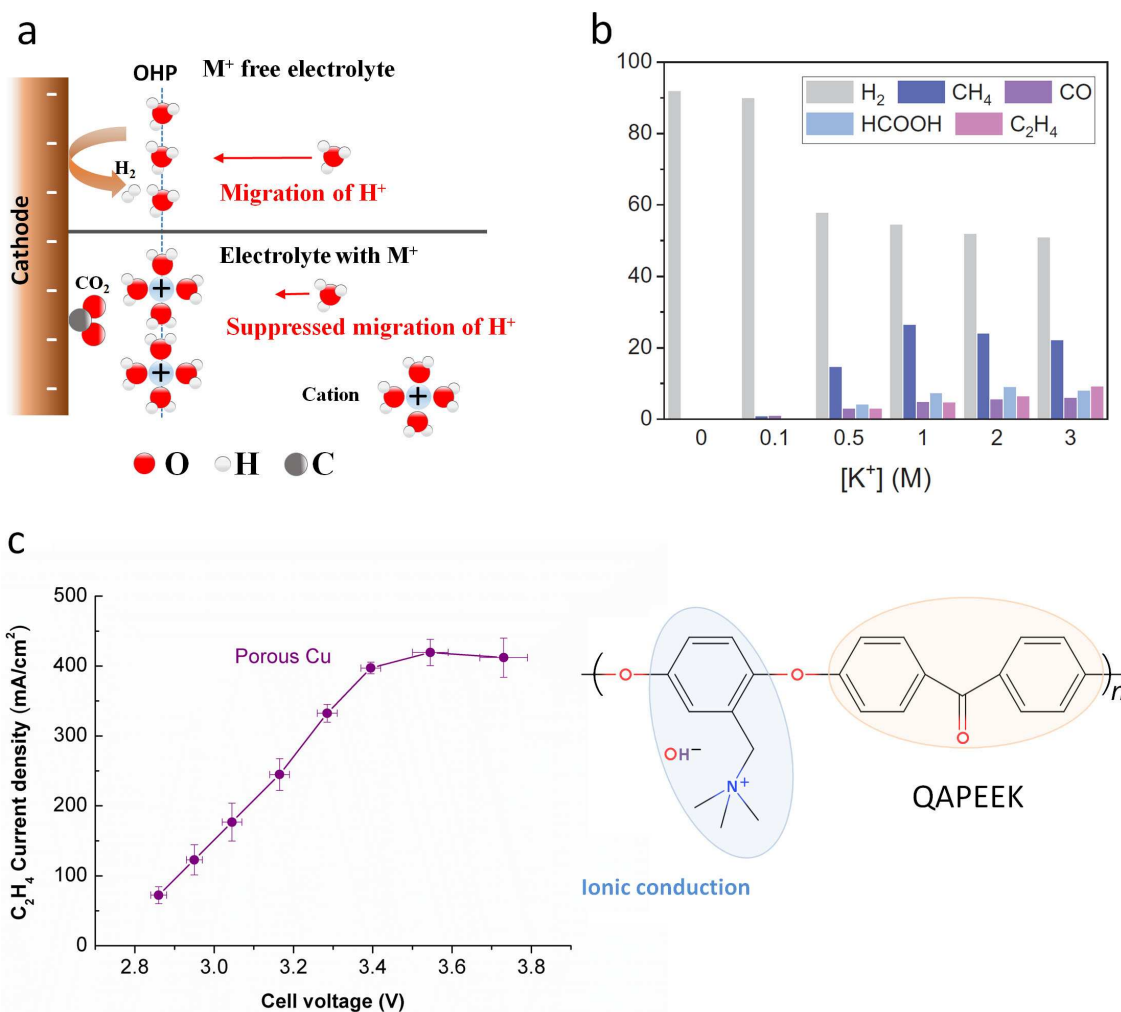


Figure 5. a), Cation effect in acidic CO_2 reduction (top: electrolyte without metal cations; bottom: electrolyte with metal cations). Figure adapted from Ref. [74]. b), Cation concentration effects in acidic CO_2 reduction. Figure adapted from permission.^[17] c), C_2H_4 current densities for porous Cu surface in CO_2 reduction at various cell potentials (left, data reproduced from Ref. [103]) and the molecular structure of QAPEEK (right).

accepted to be necessary for promoting CO_2R . Particularly, it was reported that the highly concentrated cation in the vicinity of the catalyst is capable of facilitating the selective and efficient C_{2+} formation in acid CO_2R (Figure 5b).^[17] However, beyond the activation of CO_2 and stabilization of intermediates in the presence of cation, the local pH may play a more important role in the enhanced C_{2+} formation at highly concentrated alkali cation in acidic CO_2 electrolysis. In acid, the locally neutral to basic pH conditions that favor CO_2 conversion should be created in the vicinity of the catalyst surface at a high concentration of alkali cation, owing to the local electroneutrality near the surface between the cathodic-reaction generated OH^- (equation 1) and a large amount of alkali cations. Thereby, when exploring the cation effect in acidic CO_2 reduction, it should be noted that adding H^+ may vary the local pH, which may complex the local environment factors near the cathode surface, making difficulties in disentangling a single cation effect.

3.3. Salt Precipitation

Although cations have a critical effect on the improvement in CO_2 electrolysis, a high local concentration of (bi)carbonate could be formed via the reaction of CO_2 with OH^- generated in the cathodic reactions (equation 1) at high current densities. Thus, alkali cations can precipitate in the form of alkali (bi)carbonate salts in cathodic GDEs via combining with (bi)carbonate, giving rise to flooding of GDEs and severe CO_2 mass transport limitations.^[98,99] Recently, this salt precipitation was also observed in acidic CO_2 electrolysis at high current densities,^[20,100] which may reflect that a relatively high local pH near GDE catalysts is created for electrochemically converting CO_2 in acid.

In GDE-based flowing-catholyte reactors, washing the salt precipitation using deionized water was shown to be able to restore the catalytic performance of CO_2 reduction.^[98] In addition, using a combination of highly soluble alkali cation salts^[101] with diluted cation concentrations^[102] in MEA devices is capable of circum-

venting salt precipitation that limits their long-term durability. For instance, with circulation of 10 mM KHCO_3 in anode of a MEA device, Dioxide Materials has demonstrated a remarkable stability of 3800 hours (98% CO selectivity was maintained) at 200 mA/cm^2 .^[102]

Interestingly, the Wang group reported that the use of functionalized ionomer for covering Cu surface is capable of having a cation-like function for activating CO_2 and facilitating C_{2+} formation in cation-free electrolytes.^[103] Specifically, by coating the ionically conductive QAPEEK on porous Cu surface, C_2H_4 partial current density of $>400 \text{ mA/cm}^2$ has been achieved at cell voltages of just above 3.5 V in MEA configuration with only pure water (Figure 5c).^[103] Similarly, replacing alkali cations with immobilized cationic groups such as benzimidazolium CG^[20] and a cross-linked polyelectrolyte,^[100] CO_2 reduction were also demonstrated in GDE-based flowing-catholyte reactors using metal cation-free acidic electrolyte. While it has been showed a significant progress in CO_2 electrolysis in metal cation-free electrolytes, these works do not coincide with the recent detailed fundamental work from Monteiro et al.^[72] which showed that cations are essential for CO_2 electrolysis. Thus, further work is still required to provide a more comprehensive understanding of CO_2 electrocatalysis.

4. Anion Effects

Electrolyte anions have been shown to have a considerable effect on the catalytic performance of CO_2R . The focus of most anion effects research has concentrated on tuning local pH (via distinct buffer capabilities), serving as proton and CO_2 source, modifying catalysts, as well as directly affecting intermediates formation during CO_2R (Figure 6).

4.1. Tuning Local pH

Since strong buffer anions can keep the local pH at a relatively low value via neutralizing OH^- generated in the cathodic reactions, electrolytes containing different anions that have distinct buffer strength ($\text{pKa: H}_2\text{PO}_4^- < \text{HCO}_3^- < \text{ClO}_4^-$) have been employed to modulate the local pH in CO_2R (Figure 6a).^[7,23–26] The detailed dependence of local pH on CO_2R product distributions over Cu surface is discussed in previous section.

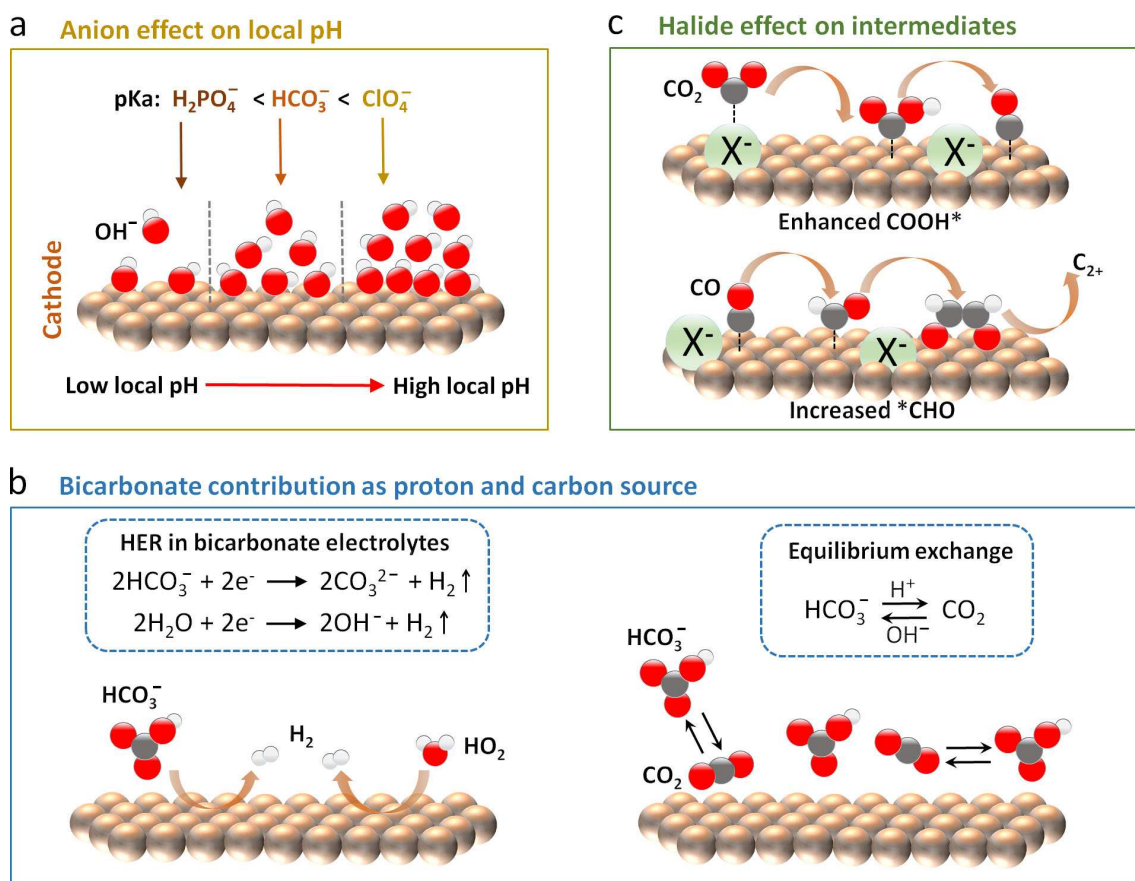


Figure 6. Anion effects in CO_2 reduction. a), Anion effect on local pH. b), Bicarbonate contribution as proton for HER (left) and carbon source for CO_2R (right). c), Halide effect on intermediates formation in CO_2R . The red, white and grey balls represent O, H and C atoms, respectively.

4.2. Serving as Proton and CO₂ Donor

As discussed in the section on local pH effects, water generally serves as the proton donor in CO₂R and HER. Of particular note, buffering anions that have lower pK_a than water also can contribute to HER as potential proton donors.^[4] For instance, in the case of the widely used bicarbonate electrolytes, proton donors for the HER pathway may be partially from bicarbonate (Figure 6b, left).^[33,34,104] CO electrolysis in KHCO₃ also revealed an apparent increase in catalytic activity of HER compared to that in alkaline electrolytes, which may be linked to that the bicarbonate also contributes proton for HER.^[40]

Additionally, while dissolved CO₂ is the carbon donor in CO₂R, Dunwell et al. has proposed that bicarbonate could increase the concentration of dissolved CO₂ in the vicinity of the cathode surface through rapid equilibrium exchange between bicarbonate and dissolved CO₂ (Figure 6b, right).^[105] Thus, bicarbonate not only works as a pH buffer but also serves a proton donor in HER and CO₂ donor in CO₂R, which complicates the role of bicarbonate during CO₂ electrolysis.

4.3. Modifying Catalysts

Utilization of anions to restructure morphology, chemical state and compositions of catalysts is an effective strategy to improve selective CO₂R.^[9,106–108] Halide ions, the most commonly used anions for modifying Cu catalysts, can be involved in the synthesis procedure in different ways. An electrochemical oxidation-reduction cycling method in the presence of halide ions has been demonstrated to restructure the Cu surface with preferential (100) facets, enhancing selectivity toward C₂H₄ and alcohols in CO₂R.^[108–112] Another way is to prepare Cu(I)-Halide and subsequent reduction of Cu(I) to Cu, and the halide-derived Cu catalysts also can result in reconstruction of Cu surface with improved C₂₊ formation.^[113–115] The enhanced C₂₊ formation via halide modification of Cu catalysts has been explained by nanostructure,^[108] grain boundaries,^[109] chemical state^[116] or even the presence of halide ions adsorbed on Cu surface.^[111,117]

4.4. Modulating Intermediates Formation

In addition to the effect of halides on the synthesis of catalysts, the presence of halide anions near the catalysts in CO₂R could also tune the formation of key intermediates in the reaction pathways, affecting the catalytic selectivity.^[117,118] Distinct theories have been proposed to elucidate the effect of halide anions on intermediates (Figure 6c). The Strasser group^[119] proposed that electronic charge donation from halide ions to Cu surface changes the local surface electronic environment, promoting certain intermediates formation in CO₂R. The charge donation of halide ions was reported to promote COOH* formation (COOH* formation is the initial step in CO₂R and requires

a relatively high activation energy barrier), thus not only lowering the overpotential in CO₂R^[120] but also increasing the population of CO adsorption that may undergo coupling.^[121] In addition, halide ions (such as fluorine) have been demonstrated to enhance hydrogenation of CO to *CHO intermediate that can form C₂₊ products.^[117]

5. Local Reactant Concentration Effects

The surface coverage of CO_x (x=1 or 2) is directly correlated with the local CO_x concentration in the vicinity of the catalyst surface.^[51,122] Thereby, tuning local CO_x concentration allows for altering surface coverage of CO_x, which may influence certain intermediates formation and corresponding reaction paths toward C₂₊ products in electrolysis.

5.1. Local CO₂ Concentration

For tuning local CO₂ concentration, several methods have been demonstrated, as shown in Figure 7a–c: (i) controlling CO₂ feed partial pressure, (ii) modulating mass transport of cathodic GDEs and (iii) changing pressure and temperature.

Since that the local CO₂ concentration is directly linked to CO₂ partial pressure on the basis of Henry's law, the effect of local reactant concentration on catalytic performance has been explored by controlling CO₂ partial pressure (Figure 7a).^[122–124] For instance, through diluting the CO₂ feed from 100 % to 25 % at 200 mA/cm², 50 % CO₂ feed was found to provide the highest C₂₊ FE while inhibiting C₁ formation, which is linked to that local CO₂ concentration when feeding the 50 % CO₂ inlet may create the more optimal coverage of CO and other intermediate species for the improved rate of C–C coupling.^[122] Thus, C–C coupling was demonstrated to be enhanced via regulating the local CO₂ availability in the vicinity of Cu surface.^[122] For achieving controllable local reactant availability, special morphology of catalysts was prepared.^[125,126] For instance, a hydrophobic Cu hierarchical structure on a GDE was prepared to provide a robust gas-liquid-solid phase, which can trap more CO₂ near Cu surface, improving C₂₊ selectivity.^[126] In addition, the composition and structure of carbon fiber substrate and microporous layer in GDEs have been shown to be able to influence mass transport of CO₂, which affects local CO₂ availability (Figure 7b), leading to variation in CO₂ performance.^[127]

Alternatively, changing pressure and temperature also could modulate local reactant concentration, although CO₂R is commonly performed at ambient pressure and temperature (Figure 7c). An enhanced CO₂ solubility can be achieved with increasing pressure or decreasing temperature,^[4] which corresponds to an increase in local CO₂ concentration. Thereby, a high pressure not only enhances the CO₂R activity, but also changes selectivity of CO₂R.^[25,128–132] A promoted C₂H₄ selectivity on Cu catalysts was found with increasing CO₂ pressure due to the improved C–C coupling at high local CO concentration (i.e. high CO coverage).^[25] Metal catalysts (such as Ag) that are inactive

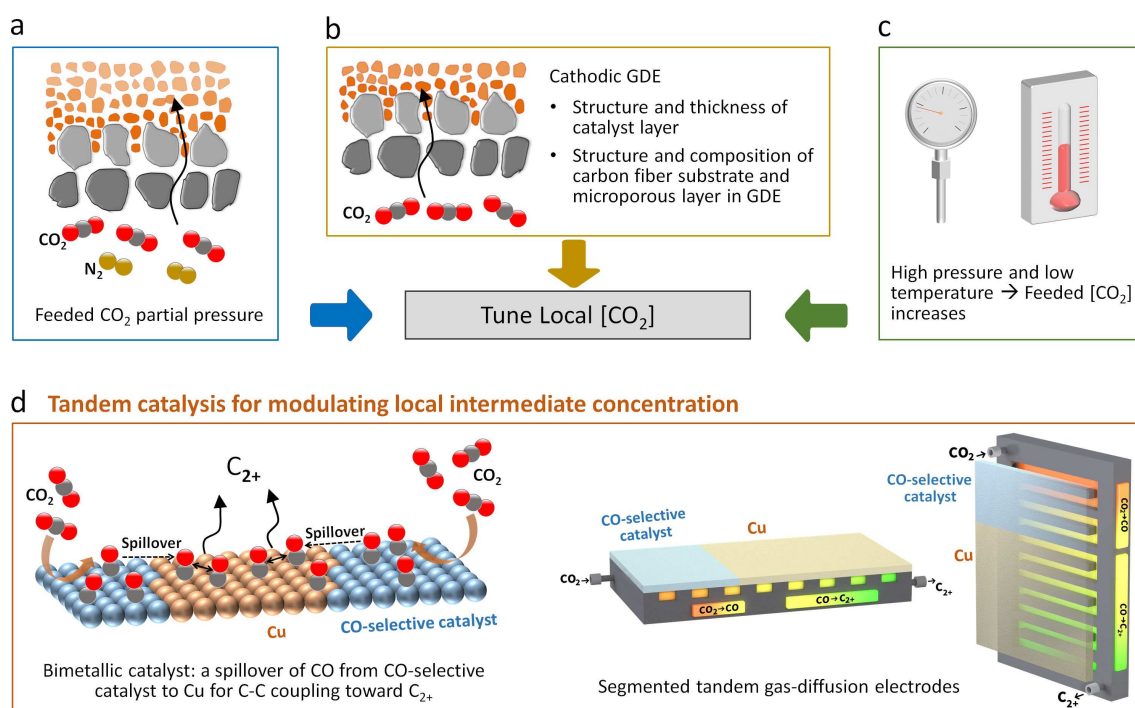


Figure 7. Local reactant concentration effects in CO_2 reduction. a), Fed CO_2 concentration effect. b), Cathodic GDE effect. c), Effect of pressure and temperature. d), Tandem catalysis for modulating local CO concentration via bimetallic catalyst (left) and segmented design (right). The red, white and grey balls represent O, H and C atoms, respectively.

for C_{2+} formation at ambient pressure exhibited Cu-like activity at an elevated pressure.^[131,133] Additionally, while decreasing temperature showed trends of suppressed H_2 evolution with enhanced CO_2R selectivity, an increased selectivity toward CH_4 was found upon lowering temperature.^[134,135] The role of temperature is still elusive due to that the temperature variation affects many factors such as CO_2 solubility, pH, electrolyte resistance, diffusion rate, and intermediates adsorption. Thus, more work needs to disentangle the temperature-induced parameters for CO_2 electrolysis.

Reactor design also plays a role in the mass transport of CO_2 that may affect local CO_2 concentration in the vicinity of the cathode surface. The flooding of cathodic GDE may occur over CO_2 electrolysis, particularly in the case of flowing-catholyte reactors (Figure 3a, left), owing to the decomposition of the hydrophobic chemical in the GDE and imbalanced pressure between catholyte and gas chamber.^[2] The water penetration into the gas chamber through the GDE could restrict the CO_2 transport to the catalyst surface (due to thick mass-transfer boundary layer^[53,136]), lowering the local CO_2 concentration near the catalyst that leads to rapid degradation in CO_2 reduction activity over electrolysis. To overcome this issue, the polytetrafluoroethylene (PTFE)-based GDE has been proposed by introducing a pure PTFE gas diffusion layer (a more stable hydrophobic layer), which can prevent flooding and achieve long-term stability (from 150 h to 2000 h) in flowing-catholyte reactors.^[76,137] In an MEA design, thousands of hours durability has been demonstrated without flooding,^[102] as

discussed in the previous section. For the most promising MEA reactors (Figure 3b, left), a flow-field design such as serpentine or parallel design not only provides an electrical contact for GDEs but also affects reactant transport. But inappropriate designs of flow fields could lead to an uneven flow distribution of reactants and uneven chemical reaction that may be linked to the durability and reliability of large-scale utilization. More details of the flow-field design of MEA configuration have been summarized in the fuel cell field.^[138]

5.2. Local CO Availability

In CO_2R , CO is a crucial intermediate for C–C coupling, and the exploration of the role of local CO concentration in C_{2+} selectivity revealed that high CO coverage favors C–C coupling toward C_{2+} products such as acetate and C_2H_4 .^[40,139] For enhancing the local CO availability, Cu-based tandem catalysis has been widely utilized (Figure 7d), whereby one CO -selective catalyst provides an in situ source of CO for C–C coupling on Cu surface.^[140–146] As the typical strategy of tandem catalysis, bimetallic catalysts are used to enhance C_{2+} products via a spillover mechanism, where CO generated on CO -selective catalyst desorbs and then migrates to nearby copper active sites for C–C coupling (Figure 7d, left).^[140–145] For instance, the group of Jaramillo^[145] showed that gold nanoparticles decorated on a Cu foil is highly active for producing alcohols, owing to that gold selectively converts CO_2 into CO to produce a high CO concentration

on nearby Cu. In addition, a segmented gas-diffusion electrode, in which an Ag segment at the inlet increases CO availability through CO₂R and a subsequent Cu segment for C–C coupling, was designed to enhance the formation of C₂₊ products (Figure 7d, right).^[146] Alternatively, a cascade strategy that couples with CO₂R to CO and COR to C₂₊ could not only enhance CO₂ utilization, as discussed in the section of local pH effects, but also provide a direct way of controlling CO concentration for improving C₂₊ formation. For achieving this goal, the direct CO-to-C₂₊ electroreduction has been explored.^[40,50,77] Recently, high-pressure CO gas (10 atm) was reported to significantly enhance CO coverage, thus reaching more than 90 % Faradaic efficiency for CO-to-acetate.^[147]

Interestingly, compared to a pure CO₂ feed and a pure CO feed, the Strasser group reported that CO₂/CO co-feeds onto Cu-based nanocatalysts could have an unexpected improvement in production of C₂H₄.^[148] Kinetic isotope-labelling experiments revealed the existence of separate and non-scrambling reactant-specific sites for CO₂ and CO, thereby the cross-coupling pathway of CO (from CO)–CO (from CO₂) facilitates the yield of C₂H₄. In addition to C₂H₄, the recent work by the Xu group showed other C₂₊ products including ethanol, n-propanol and acetate also follows the similar trend (enhanced yield) via co-feeding the mixed CO₂/CO.^[10] This work not only further confirmed the result that the existence of separated reactant-specific sites for CO₂ and CO, but also demonstrated that this cross-coupling concept is also applicable to other C₂₊ products.

6. Conclusions and Outlook

In the past decade, the focus of most CO₂R research has concentrated on the development of highly selective and active electrocatalysts for the synthesis of a specific C₂₊ product. However, the reaction process of electrocatalysis relies not only on the advanced design of the catalysts but also on the modulation of the local reaction environment near the surface of the catalysts. The selective CO₂R to C₂₊ can be significantly improved by the rational modulation of local reaction environment parameters, mainly including local pH, the species of cation and anion as well as local reactant/intermediate concentrations, as discussed in this review (Figure 1). However, there are some technical challenges, such as low carbon utilization and salt precipitation, which come with tailoring local reaction environment for high C₂₊ selectivity. These challenges need to be addressed when engineering the local reaction environment.

While substantial progress has been made in mechanistic understanding of the local factors near the catalyst surface in CO₂R through in situ and operando spectroscopy, the electrolysis process commonly involves multiple local effects that influence the final performance. Concurrently, local reaction environment factors may also lead to the variation in surface morphology, crystal facets, oxidation states or compositions of catalyst, thus the contributions from the alteration of catalysts should also be taken into account. To disentangle the local environment factors and get a better

understanding of a specific local parameter effect on C₂₊ formation, a well-defined system should be designed with isolating the effect of single local factor.

In recent years, to attain commercially relevant reaction rates, the field of CO₂ electrolysis has rapidly progressed from H-cells to GDE-type flow electrolyzers. More efforts regarding local reaction environment need to be conducted in GDE-type flow electrolyzers, which circumvents mass transport limitations, unveiling more accurate correlations between local reaction environment and catalytic selectivity. Notably, high-rate electrolysis complicates the evaluation of gaseous and liquid products, thus we proposed a benchmarking protocol for quantification of products at high-rate electrolysis,^[16,149–151] which enables us to obtain reliable catalytic trend.

The formation of C₂₊ products is a complex multistep reaction, which involves not only C₁ intermediates (such as CO) but also numerous multi-carbon intermediates. Multi-carbon intermediates have weak signals due to their low coverage, and their signals are also indistinguishable from electrolytes,^[152] thereby direct observation of the key multi-carbon intermediates with the use of in situ and operando techniques remains a challenge. It is highly desirable to develop more advanced in situ and operando techniques to provide direct evidence for reaction pathways affected by local reaction environment, simultaneously with assistance of the theoretical simulations, unveiling more reliable mechanisms. With more dedicated efforts toward local reaction environment effects, future work should switch from solely focusing on design of selective catalysts to a synergistic combination of optimizing local reaction environment and engineering catalysts for significantly facilitating the electrosynthesis of a desired product.

Acknowledgements

This work is supported by National Natural Science Foundation of China (22179105) and “Young Talent Support Plan” of Xi’an Jiaotong University (awarded to M.M.). This work was also supported by the Villum Center for the Science of Sustainable Fuels and Chemical grant 9455 (VSustain). We thank Dr. Jia Liu at Instrumental Analysis Center of Xi’an Jiaotong University for discussing the spectroscopy techniques.

Conflict of Interest

The authors declare no conflict of interest.

Data Availability Statement

Data sharing is not applicable to this article as no new data were created or analyzed in this study.

Keywords: CO₂ reduction • multicarbon products • catalytic selectivity • local reaction environment • C–C coupling

- [1] E. W. Lees, B. A. W. Mowbray, F. G. L. Parlane, C. P. Berlinguette, *Nat. Rev. Mater.* **2021**, *7*, 55–64.
- [2] D. Wakerley, S. Lamaison, J. Wicks, A. Clemens, J. Feaster, D. Corral, S. A. Jaffer, A. Sarkar, M. Fontecave, E. B. Duoss, S. Baker, E. H. Sargent, T. F. Jaramillo, C. Hahn, *Nat. Energy* **2022**, *7*, 130–143.
- [3] Y. Y. Birdja, E. Pérez-Gallent, M. C. Figueiredo, A. J. Göttle, F. Calle-Vallejo, M. T. M. Koper, *Nat. Energy* **2019**, *4*, 732–745.
- [4] S. Nitopi, E. Bertheussen, S. B. Scott, X. Liu, A. K. Engstfeld, S. Horch, B. Seger, I. E. L. Stephens, K. Chan, C. Hahn, J. K. Nørskov, T. F. Jaramillo, I. Chorkendorff, *Chem. Rev.* **2019**, *119*, 7610–7672.
- [5] D. Gao, R. M. Arán-Ais, H. S. Jeon, B. Roldan Cuenya, *Nat. Catal.* **2019**, *2*, 198–210.
- [6] Y. Yang, S. Louisia, S. Yu, J. Jin, I. Roh, C. Chen, M. V. Fonseca Guzman, J. Feijóo, P. C. Chen, H. Wang, C. J. Pollock, X. Huang, Y. T. Shao, C. Wang, D. A. Muller, H. D. Abruña, P. Yang, *Nature* **2023**, *614*, 262–269.
- [7] M. Ma, K. Djanashvili, W. A. Smith, *Angew. Chem. Int. Ed.* **2016**, *55*, 6680–6684.
- [8] C. W. Li, J. Ciston, M. W. Kanan, *Nature* **2014**, *508*, 504–507.
- [9] D. Zhong, Z. Zhao, Q. Zhao, D. Cheng, B. Liu, G. Zhang, W. Deng, H. Dong, L. Zhang, J. Li, J. Li, J. Gong, *Angew. Chem. Int. Ed.* **2021**, *60*, 4879–4885.
- [10] W. Gao, Y. Xu, L. Fu, X. Chang, B. Xu, *Nat. Catal.* **2023**, *6*, 885–894.
- [11] H. Mistry, A. S. Varela, C. S. Bonifacio, I. Zegkinoglou, I. Sinev, Y.-W. Choi, K. Kisslinger, E. A. Stach, J. C. Yang, P. Strasser, B. R. Cuenya, *Nat. Commun.* **2016**, *7*, 12123.
- [12] P. De Luna, R. Quintero-Bermudez, C.-T. Dinh, M. B. Ross, O. S. Bushuyev, P. Todorović, T. Regier, S. O. Kelley, P. Yang, E. H. Sargent, *Nat. Catal.* **2018**, *1*, 103–110.
- [13] S. Ma, M. Sadakiyo, M. Heima, R. Luo, R. T. Haasch, J. I. Gold, M. Yamauchi, P. J. A. Kenis, *J. Am. Chem. Soc.* **2017**, *139*, 47–50.
- [14] M. Zhong, K. Tran, Y. Min, C. Wang, Z. Wang, C.-T. Dinh, P. De Luna, Z. Yu, A. S. Rasouli, P. Brodersen, S. Sun, O. Voznyy, C.-S. Tan, M. Askerka, F. Che, M. Liu, A. Seifitokaldani, Y. Pang, S.-C. Lo, A. Ip, Z. Ulissi, E. H. Sargent, *Nature* **2020**, *581*, 178–183.
- [15] X. Wang, Z. Wang, F. P. García de Arquer, C.-T. Dinh, A. Ozden, Y. C. Li, D.-H. Nam, J. Li, Y.-S. Liu, J. Wicks, Z. Chen, M. Chi, B. Chen, Y. Wang, J. Tam, J. Y. Howe, A. Proppe, P. Todorović, F. Li, T.-T. Zhuang, C. M. Gabardo, A. R. Kirmani, C. McCallum, S.-F. Hung, Y. Lum, M. Luo, Y. Min, A. Xu, C. P. O'Brien, B. Stephen, B. Sun, A. H. Ip, L. J. Richter, S. O. Kelley, D. Sinton, E. H. Sargent, *Nat. Energy* **2020**, *5*, 478–486.
- [16] M. Ma, E. L. Clark, K. T. Therkildsen, S. Dalsgaard, I. Chorkendorff, B. Seger, *Energy Environ. Sci.* **2020**, *13*, 977–985.
- [17] J. E. Huang, F. Li, A. Ozden, A. Sedighian Rasouli, F. P. García de Arquer, S. Liu, S. Zhang, M. Luo, X. Wang, Y. Lum, Y. Xu, K. Bertens, R. K. Miao, C.-T. Dinh, D. Sinton, E. H. Sargent, *Science (80-)* **2021**, *372*, 1074–1078.
- [18] Y. Xie, P. Ou, X. Wang, Z. Xu, Y. C. Li, Z. Wang, J. E. Huang, J. Wicks, C. McCallum, N. Wang, Y. Wang, T. Chen, B. T. W. Lo, D. Sinton, J. C. Yu, Y. Wang, E. H. Sargent, *Nat. Catal.* **2022**, *5*, 564–570.
- [19] Y. Zhao, L. Hao, A. Ozden, S. Liu, R. K. Miao, P. Ou, T. Alkayyali, S. Zhang, J. Ning, Y. Liang, Y. Xu, M. Fan, Y. Chen, J. E. Huang, K. Xie, J. Zhang, C. P. O'Brien, F. Li, E. H. Sargent, D. Sinton, *Nat. Synth.* **2023**, *2*, 403–412.
- [20] M. Fan, J. E. Huang, R. K. Miao, Y. Mao, P. Ou, F. Li, X.-Y. Li, Y. Cao, Z. Zhang, J. Zhang, Y. Yan, A. Ozden, W. Ni, Y. Wang, Y. Zhao, Z. Chen, B. Khatir, C. P. O'Brien, Y. Xu, Y. C. Xiao, G. I. N. Waterhouse, K. Golovin, Z. Wang, E. H. Sargent, D. Sinton, *Nat. Catal.* **2023**, *6*, 763–772.
- [21] H. Shin, K. U. Hansen, F. Jiao, *Nat. Sustain.* **2021**, *4*, 911–919.
- [22] A. Wagner, C. D. Sahn, E. Reisner, *Nat. Catal.* **2020**, *3*, 775–786.
- [23] Y. Hori, A. Murata, R. Takahashi, *J. Chem. Soc. Faraday Trans. 1 Phys. Chem. Condens. Phases* **1989**, *85*, 2309.
- [24] Y. Hori, in *Mod. Asp. Electrochem.* (Ed.: E. Vayenas, C. G., White, R. E., Gamboa-Aldeco, M. E.), Springer New York, New York, NY, **2004**, pp. 89–189.
- [25] R. Kas, R. Kortlever, H. Yilmaz, M. T. M. Koper, G. Mul, *ChemElectroChem* **2015**, *2*, 354–358.
- [26] A. S. Varela, M. Kroschel, T. Reier, P. Strasser, *Catal. Today* **2016**, *260*, 8–13.
- [27] R. Kas, R. Kortlever, A. Milbrat, M. T. M. Koper, G. Mul, J. Baltrusaitis, *Phys. Chem. Chem. Phys.* **2014**, *16*, 12194.
- [28] M. Ma, B. J. Trzeźniewski, J. Xie, W. A. Smith, *Angew. Chem. Int. Ed.* **2016**, *55*, 9748–9752.
- [29] W. Luo, J. Zhang, M. Li, A. Züttel, *ACS Catal.* **2019**, *9*, 3783–3791.
- [30] C. F. C. Lim, D. A. Harrington, A. T. Marshall, *Electrochim. Acta* **2017**, *238*, 56–63.
- [31] H. Ooka, M. C. Figueiredo, M. T. M. Koper, *Langmuir* **2017**, *33*, 9307–9313.
- [32] Y. Yoon, A. S. Hall, Y. Surendranath, *Angew. Chem. Int. Ed.* **2016**, *55*, 15282–15286.
- [33] A. Goyal, G. Marcandalli, V. A. Mints, M. T. M. Koper, *J. Am. Chem. Soc.* **2020**, *142*, 4154–4161.
- [34] G. Marcandalli, A. Goyal, M. T. M. Koper, *ACS Catal.* **2021**, *11*, 4936–4945.
- [35] A. Goyal, M. T. M. Koper, *J. Chem. Phys.* **2021**, *155*, 134705.
- [36] E. W. Lees, B. A. W. Mowbray, D. A. Salvatore, G. L. Simpson, D. J. Dvorak, S. Ren, J. Chau, K. L. Milton, C. P. Berlinguette, *J. Mater. Chem. A* **2020**, *8*, 19493–19501.
- [37] C. Kim, J. C. Bui, X. Luo, J. K. Cooper, A. Kusoglu, A. Z. Weber, A. T. Bell, *Nat. Energy* **2021**, *6*, 1026–1034.
- [38] Y. Zhao, X. Zu, R. Chen, X. Li, Y. Jiang, Z. Wang, S. Wang, Y. Wu, Y. Sun, Y. Xie, *J. Am. Chem. Soc.* **2022**, *144*, 10446–10454.
- [39] J. C. Bui, C. Kim, A. J. King, O. Romiluyi, A. Kusoglu, A. Z. Weber, A. T. Bell, *Acc. Chem. Res.* **2022**, *55*, 484–494.
- [40] M. Ma, W. Deng, A. Xu, D. Hochfilzer, Y. Qiao, K. Chan, I. Chorkendorff, B. Seger, *Energy Environ. Sci.* **2022**, *15*, 2470–2478.
- [41] Y. Hori, A. Murata, R. Takahashi, S. Suzuki, *J. Am. Chem. Soc.* **1988**, *109*, 17.
- [42] A. Murata, Y. Hori, *Bull. Chem. Soc. Jpn.* **1991**, *64*, 123–127.
- [43] Y. Hori, R. Takahashi, Y. Yoshinami, A. Murata, *J. Phys. Chem. B* **1997**, *101*, 7075–7081.
- [44] L. Wang, S. A. Nitopi, E. Bertheussen, M. Orazov, C. G. Morales-Guio, X. Liu, D. C. Higgins, K. Chan, J. K. Nørskov, C. Hahn, T. F. Jaramillo, *ACS Catal.* **2018**, *8*, 7445–7454.
- [45] K. J. P. Schouten, Y. Kwon, C. J. M. van der Ham, Z. Qin, M. T. M. Koper, *Chem. Sci.* **2011**, *2*, 1902.
- [46] K. J. P. Schouten, Z. Qin, E. Pérez Gallent, M. T. M. Koper, *J. Am. Chem. Soc.* **2012**, *134*, 9864–9867.
- [47] F. Calle-Vallejo, M. T. M. Koper, *Angew. Chem.* **2013**, *125*, 7423–7426.
- [48] K. J. P. Schouten, E. Pérez Gallent, M. T. M. Koper, *J. Electroanal. Chem.* **2014**, *716*, 53–57.
- [49] J. Li, X. Chang, H. Zhang, A. S. Malkani, M. Cheng, B. Xu, Q. Lu, *Nat. Commun.* **2021**, *12*, 3264.

- [50] M. Jouny, W. Luc, F. Jiao, *Nat. Catal.* **2018**, *1*, 748–755.
- [51] J. Li, Z. Wang, C. McCallum, Y. Xu, F. Li, Y. Wang, C. M. Gabardo, C.-T. Dinh, T.-T. Zhuang, L. Wang, J. Y. Howe, Y. Ren, E. H. Sargent, D. Sinton, *Nat. Catal.* **2019**, *2*, 1124–1131.
- [52] T. Burdyny, W. A. Smith, *Energy Environ. Sci.* **2019**, *12*, 1442–1453.
- [53] L.-C. Weng, A. T. Bell, A. Z. Weber, *Phys. Chem. Chem. Phys.* **2018**, *20*, 16973–16984.
- [54] G. Kastlunger, H. Heenen, N. Govindarajan, *ACS Catal.* **2023**, *13*, 5062–5072.
- [55] Y. Qiao, D. Hochfilzer, J. Kibsgaard, I. Chorkendorff, B. Seger, *ACS Energy Lett.* **2024**, *9*, 880–887.
- [56] Y. Y. Birdja, M. T. M. Koper, *J. Am. Chem. Soc.* **2017**, *139*, 2030–2034.
- [57] J. Andraos, A. J. Kresge, *Can. J. Chem.* **2000**, *78*, 508–515.
- [58] Y. Chiang, A. J. Kresge, V. V. Popik, *J. Chem. Soc.-Perkin Trans.* **1999**, *2*, 1107–1110.
- [59] W. Luc, X. Fu, J. Shi, J.-J. Lv, M. Jouny, B. H. Ko, Y. Xu, Q. Tu, X. Hu, J. Wu, Q. Yue, Y. Liu, F. Jiao, Y. Kang, *Nat. Catal.* **2019**, *2*, 423–430.
- [60] M. Jouny, J.-J. Lv, T. Cheng, B. H. Ko, J.-J. Zhu, W. A. Goddard, F. Jiao, *Nat. Chem.* **2019**, *11*, 846–851.
- [61] T. Wu, H. Bu, S. Tao, M. Ma, *Nanoscale* **2024**, *16*, 3926–3935.
- [62] N. Gupta, M. Gattrell, B. MacDougall, *J. Appl. Electrochem.* **2005**, *36*, 161–172.
- [63] A. Böhme, J. C. Bui, A. Q. Fenwick, R. Bhide, C. N. Feltenberger, A. J. Welch, A. J. King, A. T. Bell, A. Z. Weber, S. Ardo, H. A. Atwater, *Energy Environ. Sci.* **2023**, *16*, 1783–1795.
- [64] O. Ayemoba, A. Cuesta, *ACS Appl. Mater. Interfaces* **2017**, *9*, 27377–27382.
- [65] K. Yang, R. Kas, W. A. Smith, *J. Am. Chem. Soc.* **2019**, *141*, 15891–15900.
- [66] D. A. Henckel, M. J. Counihan, H. E. Holmes, X. Chen, U. O. Nwabara, S. Verma, J. Rodríguez-López, P. J. A. Kenis, A. A. Gewirth, *ACS Catal.* **2021**, *11*, 255–263.
- [67] Z. Zhang, L. Melo, R. P. Janssonius, F. Habibzadeh, E. R. Grant, C. P. Berlinguette, *ACS Energy Lett.* **2020**, *5*, 3101–3107.
- [68] X. Lu, C. Zhu, Z. Wu, J. Xuan, J. S. Francisco, H. Wang, *J. Am. Chem. Soc.* **2020**, *142*, 15438–15444.
- [69] Y. N. Xu, W. Li, H. Q. Fu, X. Y. Zhang, J. Y. Zhao, X. Wu, H. Y. Yuan, M. Zhu, S. Dai, P. F. Liu, H. G. Yang, *Angew. Chem. Int. Ed.* **2023**, *62*, DOI 10.1002/anie.202217296.
- [70] F. Zhang, A. C. Co, *Angew. Chem. Int. Ed.* **2020**, *59*, 1674–1681.
- [71] M. C. O. Monteiro, A. Mirabal, L. Jacobse, K. Doblhoff-Dier, S. C. Barton, M. T. M. Koper, *JACS Au* **2021**, *1*, 1915–1924.
- [72] M. C. O. Monteiro, F. Dattila, B. Hagedoorn, R. García-Muelas, N. López, M. T. M. Koper, *Nat. Catal.* **2021**, *4*, 654–662.
- [73] W. Deng, P. Zhang, B. Seger, J. Gong, *Nat. Commun.* **2022**, *13*, 803.
- [74] J. Gu, S. Liu, W. Ni, W. Ren, S. Haussener, X. Hu, *Nat. Catal.* **2022**, *5*, 268–276.
- [75] C. J. Bondue, M. Graf, A. Goyal, M. T. M. Koper, *J. Am. Chem. Soc.* **2021**, *143*, 279–285.
- [76] C.-T. Dinh, T. Burdyny, M. G. Kibria, A. Seifitokaldani, C. M. Gabardo, F. P. García de Arquer, A. Kiani, J. P. Edwards, P. De Luna, O. S. Bushuyev, C. Zou, R. Quintero-Bermudez, Y. Pang, D. Sinton, E. H. Sargent, *Science (80-)* **2018**, *360*, 783–787.
- [77] M. Jouny, G. S. Hutchings, F. Jiao, *Nat. Catal.* **2019**, *2*, 1062–1070.
- [78] A. Ozden, F. P. García de Arquer, J. E. Huang, J. Wicks, J. Sisler, R. K. Miao, C. P. O'Brien, G. Lee, X. Wang, A. H. Ip, E. H. Sargent, D. Sinton, *Nat. Sustain.* **2022**, *5*, 563–573.
- [79] J. A. Rabinowitz, M. W. Kanan, *Nat. Commun.* **2020**, *11*, 5231.
- [80] M. Ma, S. Kim, I. Chorkendorff, B. Seger, *Chem. Sci.* **2020**, *11*, 8854–8861.
- [81] K. Xie, R. K. Miao, A. Ozden, S. Liu, Z. Chen, C.-T. Dinh, J. E. Huang, Q. Xu, C. M. Gabardo, G. Lee, J. P. Edwards, C. P. O'Brien, S. W. Boettcher, D. Sinton, E. H. Sargent, *Nat. Commun.* **2022**, *13*, 3609.
- [82] J. Y. 'Timothy' Kim, P. Zhu, F.-Y. Chen, Z.-Y. Wu, D. A. Cullen, H. Wang, *Nat. Catal.* **2022**, *5*, 288–299.
- [83] J. Fan, B. Pan, J. Wu, C. Shao, Z. Wen, Y. Yan, Y. Wang, Y. Li, *Angew. Chem. Int. Ed.* **2024**, *63*, 1–6.
- [84] A. Ozden, Y. Wang, F. Li, M. Luo, J. Sisler, A. Thevenon, A. Rosas-Hernández, T. Burdyny, Y. Lum, H. Yadegari, T. Agapie, J. C. Peters, E. H. Sargent, D. Sinton, *Joule* **2021**, *5*, 706–719.
- [85] C. Delacourt, P. L. Ridgway, J. B. Kerr, J. Newman, *J. Electrochem. Soc.* **2008**, *155*, B42.
- [86] M. M. Waegle, C. M. Gunathunge, J. Li, X. Li, *J. Chem. Phys.* **2019**, *151*, 160902.
- [87] M. R. Singh, Y. Kwon, Y. Lum, J. W. Ager, A. T. Bell, *J. Am. Chem. Soc.* **2016**, *138*, 13006–13012.
- [88] A. S. Malkani, J. Anibal, B. Xu, *ACS Catal.* **2020**, *10*, 14871–14876.
- [89] S. A. Akhade, I. T. McCrum, M. J. Janik, *J. Electrochem. Soc.* **2016**, *163*, F477–F484.
- [90] C. M. Gunathunge, V. J. Ovalle, M. M. Waegle, *Phys. Chem. Chem. Phys.* **2017**, *19*, 30166–30172.
- [91] L. D. Chen, M. Urushihara, K. Chan, J. K. Nørskov, *ACS Catal.* **2016**, *6*, 7133–7139.
- [92] J. Resasco, L. D. Chen, E. Clark, C. Tsai, C. Hahn, T. F. Jaramillo, K. Chan, A. T. Bell, *J. Am. Chem. Soc.* **2017**, *139*, 11277–11287.
- [93] S. Ringe, E. L. Clark, J. Resasco, A. Walton, B. Seger, A. T. Bell, K. Chan, *Energy Environ. Sci.* **2019**, *12*, 3001–3014.
- [94] V. J. Ovalle, Y.-S. Hsu, N. Agrawal, M. J. Janik, M. M. Waegle, *Nat. Catal.* **2022**, *5*, 624–632.
- [95] J. Li, D. Wu, A. S. Malkani, X. Chang, M. Cheng, B. Xu, Q. Lu, *Angew. Chem.* **2020**, *132*, 4494–4499.
- [96] D. Gao, I. T. McCrum, S. Deo, Y.-W. Choi, F. Scholten, W. Wan, J. G. Chen, M. J. Janik, B. Roldan Cuenya, *ACS Catal.* **2018**, *8*, 10012–10020.
- [97] Y. Qiao, W. Lai, K. Huang, T. Yu, Q. Wang, L. Gao, Z. Yang, Z. Ma, T. Sun, M. Liu, C. Lian, H. Huang, *ACS Catal.* **2022**, *12*, 2357–2364.
- [98] S. Verma, Y. Hamasaki, C. Kim, W. Huang, S. Lu, H.-R. M. Jhong, A. A. Gewirth, T. Fujigaya, N. Nakashima, P. J. A. Kenis, *ACS Energy Lett.* **2018**, *3*, 193–198.
- [99] M. Sassenburg, M. Kelly, S. Subramanian, W. A. Smith, T. Burdyny, *ACS Energy Lett.* **2023**, *8*, 321–331.
- [100] H.-G. Qin, Y.-F. Du, Y.-Y. Bai, F.-Z. Li, X. Yue, H. Wang, J.-Z. Peng, J. Gu, *Nat. Commun.* **2023**, *14*, 5640.
- [101] S. Garg, Q. Xu, A. B. Moss, M. Mirolu, W. Deng, I. Chorkendorff, J. Drnec, B. Seger, *Energy Environ. Sci.* **2023**, *16*, 1631–1643.
- [102] Z. Liu, H. Yang, R. Kutz, R. I. Masel, *J. Electrochem. Soc.* **2018**, *165*, J3371–J3377.
- [103] W. Li, Z. Yin, Z. Gao, G. Wang, Z. Li, F. Wei, X. Wei, H. Peng, X. Hu, L. Xiao, J. Lu, L. Zhuang, *Nat. Energy* **2022**, *7*, 835–843.
- [104] A. Wuttig, M. Yaguchi, K. Motobayashi, M. Osawa, Y. Surendranath, *Proc. Nat. Acad. Sci.* **2016**, *113*, E4585–E4593.
- [105] M. Dunwell, Q. Lu, J. M. Heyes, J. Rosen, J. G. Chen, Y. Yan, F. Jiao, B. Xu, *J. Am. Chem. Soc.* **2017**, *139*, 3774–3783.
- [106] Y.-C. Hsieh, S. D. Senanayake, Y. Zhang, W. Xu, D. E. Polyansky, *ACS Catal.* **2015**, *5*, 5349–5356.

- [107] M. Ma, K. Liu, J. Shen, R. Kas, W. A. Smith, *ACS Energy Lett.* **2018**, *3*, 1301–1306.
- [108] F. S. Roberts, K. P. Kuhl, A. Nilsson, *Angew. Chem. Int. Ed.* **2015**, *54*, 5179–5182.
- [109] Y. Kwon, Y. Lum, E. L. Clark, J. W. Ager, A. T. Bell, *ChemElectroChem* **2016**, *3*, 1012–1019.
- [110] D. Gao, I. Zegkinoglou, N. J. Divins, F. Scholten, I. Sinev, P. Grosse, B. Roldan Cuenya, *ACS Nano* **2017**, *11*, 4825–4831.
- [111] D. Gao, I. Sinev, F. Scholten, R. M. Arán-Ais, N. J. Divins, K. Kvashnina, J. Timoshenko, B. Roldan Cuenya, *Angew. Chem. Int. Ed.* **2019**, *58*, 17047–17053.
- [112] J. Han, C. Long, J. Zhang, K. Hou, Y. Yuan, D. Wang, X. Zhang, X. Qiu, Y. Zhu, Y. Zhang, Z. Yang, S. Yan, Z. Tang, *Chem. Sci.* **2020**, *11*, 10698–10704.
- [113] M. G. Kibria, C.-T. Dinh, A. Seifitokaldani, P. De Luna, T. Burdyny, R. Quintero-Bermudez, M. B. Ross, O. S. Bushuyev, F. P. García de Arquer, P. Yang, D. Sinton, E. H. Sargent, *Adv. Mater.* **2018**, *30*, 1804867.
- [114] H. Wang, E. Matios, C. Wang, J. Luo, X. Lu, X. Hu, W. Li, *Nano Lett.* **2019**, *19*, 3925–3932.
- [115] T. Kim, G. T. R. Palmore, *Nat. Commun.* **2020**, *11*, 3622.
- [116] M. Li, Y. Ma, J. Chen, R. Lawrence, W. Luo, M. Sacchi, W. Jiang, J. Yang, *Angew. Chem. Int. Ed.* **2021**, *60*, 11487–11493.
- [117] W. Ma, S. Xie, T. Liu, Q. Fan, J. Ye, F. Sun, Z. Jiang, Q. Zhang, J. Cheng, Y. Wang, *Nat. Catal.* **2020**, *3*, 478–487.
- [118] F. Quan, D. Zhong, H. Song, F. Jia, L. Zhang, *J. Mater. Chem. A* **2015**, *3*, 16409–16413.
- [119] A. S. Varela, W. Ju, T. Reier, P. Strasser, *ACS Catal.* **2016**, *6*, 2136–2144.
- [120] D. Gao, F. Scholten, B. Roldan Cuenya, *ACS Catal.* **2017**, *7*, 5112–5120.
- [121] Y. Huang, C. W. Ong, B. S. Yeo, *ChemSusChem* **2018**, *11*, 3299–3306.
- [122] Y. C. Tan, K. B. Lee, H. Song, J. Oh, *Joule* **2020**, *4*, 1104–1120.
- [123] G. Z. Kyriacou, A. K. Anagnostopoulos, *J. Appl. Electrochem.* **1993**, *23*, 483–486.
- [124] B. Kim, S. Ma, H.-R. Molly Jhong, P. J. A. Kenis, *Electrochim. Acta* **2015**, *166*, 271–276.
- [125] M. Liu, Y. Pang, B. Zhang, P. De Luna, O. Voznyy, J. Xu, X. Zheng, C. T. Dinh, F. Fan, C. Cao, F. P. G. de Arquer, T. S. Safaei, A. Mepham, A. Klinkova, E. Kumacheva, T. Filleter, D. Sinton, S. O. Kelley, E. H. Sargent, *Nature* **2016**, *537*, 382–386.
- [126] Z.-Z. Niu, F.-Y. Gao, X.-L. Zhang, P.-P. Yang, R. Liu, L.-P. Chi, Z.-Z. Wu, S. Qin, X. Yu, M.-R. Gao, *J. Am. Chem. Soc.* **2021**, *143*, 8011–8021.
- [127] B. Kim, F. Hillman, M. Ariyoshi, S. Fujikawa, P. J. A. Kenis, *J. Power Sources* **2016**, *312*, 192–198.
- [128] E. J. Dufek, T. E. Lister, S. G. Stone, M. E. McIlwain, *J. Electrochem. Soc.* **2012**, *159*, F514–F517.
- [129] C. M. Gabardo, A. Seifitokaldani, J. P. Edwards, C.-T. Dinh, T. Burdyny, M. G. Kibria, C. P. O'Brien, E. H. Sargent, D. Sinton, *Energy Environ. Sci.* **2018**, *11*, 2531–2539.
- [130] M. Ramdin, A. R. T. Morrison, M. de Groen, R. van Haperen, R. de Kler, L. J. P. van den Broeke, J. P. M. Trusler, W. de Jong, T. J. H. Vlught, *Ind. Eng. Chem. Res.* **2019**, *58*, 1834–1847.
- [131] S. J. Raaijman, M. P. Schellekens, P. J. Corbett, M. T. M. Koper, *Angew. Chem. Int. Ed.* **2021**, *60*, 21732–21736.
- [132] L. Huang, G. Gao, C. Yang, X. Li, R. K. Miao, Y. Xue, K. Xie, P. Ou, C. T. Yavuz, Y. Han, G. Magnotti, D. Sinton, E. H. Sargent, X. Lu, *Nat. Commun.* **2023**, *14*, 2958.
- [133] A. Kudo, S. Nakagawa, A. Tsuneto, T. Sakata, *J. Electrochem. Soc.* **1993**, *140*, 1541–1545.
- [134] Y. Hori, K. Kikuchi, A. Murata, S. Suzuki, *Chem. Lett.* **1986**, 897–898.
- [135] S. T. Ahn, I. Abu-Baker, G. T. R. Palmore, *Catal. Today* **2017**, *288*, 24–29.
- [136] L. Xue, X. Wu, Y. Liu, B. Xu, X. Wang, S. Dai, P. Liu, H. Yang, *Nano Res.* **2022**, *15*, 1393–1398.
- [137] W. Fang, W. Guo, R. Lu, Y. Yan, X. Liu, D. Wu, F. M. Li, Y. Zhou, C. He, C. Xia, H. Niu, S. Wang, Y. Liu, Y. Mao, C. Zhang, B. You, Y. Pang, L. Duan, X. Yang, F. Song, T. Zhai, G. Wang, X. Guo, B. Tan, T. Yao, Z. Wang, B. Y. Xia, *Nature* **2024**, *626*, 86–91.
- [138] J. Wang, *Appl. Energy* **2015**, *157*, 640–663.
- [139] Y. Ji, Z. Chen, R. Wei, C. Yang, Y. Wang, J. Xu, H. Zhang, A. Guan, J. Chen, T.-K. Sham, J. Luo, Y. Yang, X. Xu, G. Zheng, *Nat. Catal.* **2022**, *5*, 251–258.
- [140] J. Huang, M. Mensi, E. Oveisi, V. Mantella, R. Buonsanti, *J. Am. Chem. Soc.* **2019**, *141*, 2490–2499.
- [141] D. Ren, B. S. H. Ang, B. S. Yeo, *ACS Catal.* **2016**, *6*, 8239–8247.
- [142] E. L. Clark, C. Hahn, T. F. Jaramillo, A. T. Bell, *J. Am. Chem. Soc.* **2017**, *139*, 15848–15857.
- [143] S. Lee, G. Park, J. Lee, *ACS Catal.* **2017**, *7*, 8594–8604.
- [144] Y. Lum, J. W. Ager, *Energy Environ. Sci.* **2018**, *11*, 2935–2944.
- [145] C. G. Morales-Guio, E. R. Cave, S. A. Nitopi, J. T. Feaster, L. Wang, K. P. Kuhl, A. Jackson, N. C. Johnson, D. N. Abram, T. Hatsukade, C. Hahn, T. F. Jaramillo, *Nat. Catal.* **2018**, *1*, 764–771.
- [146] T. Zhang, J. C. Bui, Z. Li, A. T. Bell, A. Z. Weber, J. Wu, *Nat. Catal.* **2022**, *5*, 202–211.
- [147] J. Jin, J. Wicks, Q. Min, J. Li, Y. Hu, J. Ma, Y. Wang, Z. Jiang, Y. Xu, R. Lu, G. Si, P. Papangelakis, M. Shakouri, Q. Xiao, P. Ou, X. Wang, Z. Chen, W. Zhang, K. Yu, J. Song, X. Jiang, P. Qiu, Y. Lou, D. Wu, Y. Mao, A. Ozden, C. Wang, B. Y. Xia, X. Hu, V. P. Dravid, Y.-M. Yiu, T.-K. Sham, Z. Wang, D. Sinton, L. Mai, E. H. Sargent, Y. Pang, *Nature* **2023**, *617*, 724–729.
- [148] X. Wang, J. F. de Araújo, W. Ju, A. Bagger, H. Schmies, S. Kühn, J. Rossmeisl, P. Strasser, *Nat. Nanotechnol.* **2019**, *14*, 1063–1070.
- [149] M. Ma, Z. Zheng, W. Yan, C. Hu, B. Seger, *ACS Energy Lett.* **2022**, *7*, 2595–2601.
- [150] B. Seger, M. Robert, F. Jiao, *Nat. Sustain.* **2023**, *6*, 236–238.
- [151] Q. Xu, S. Liu, F. Longhin, G. Kastlunger, I. Chorkendorff, B. Seger, *Adv. Mater.* **2023**, *2306741*, 1–11.
- [152] I. E. L. Stephens, K. Chan, A. Bagger, S. W. Boettcher, J. Bonin, E. Boutin, A. K. Buckley, R. Buonsanti, E. R. Cave, X. Chang, S. W. Chee, A. H. M. da Silva, P. de Luna, O. Einsle, B. Endrődi, M. Escudero-Escribano, J. V. Ferreira de Araujo, M. C. Figueiredo, C. Hahn, K. U. Hansen, S. Haussener, S. Hunegnaw, Z. Huo, Y. J. Hwang, C. Janáky, B. S. Jayatilake, F. Jiao, Z. P. Jovanov, P. Karimi, M. T. M. Koper, K. P. Kuhl, W. H. Lee, Z. Liang, X. Liu, S. Ma, M. Ma, H. Oh, M. Robert, B. R. Cuenya, J. Rossmeisl, C. Roy, M. P. Ryan, E. H. Sargent, P. Sebastián-Pascual, B. Seger, L. Steier, P. Strasser, A. S. Varela, R. E. Vos, X. Wang, B. Xu, H. Yadegari, Y. Zhou, *J. Phys. E* **2022**, *4*, 042003.

Manuscript received: January 17, 2024

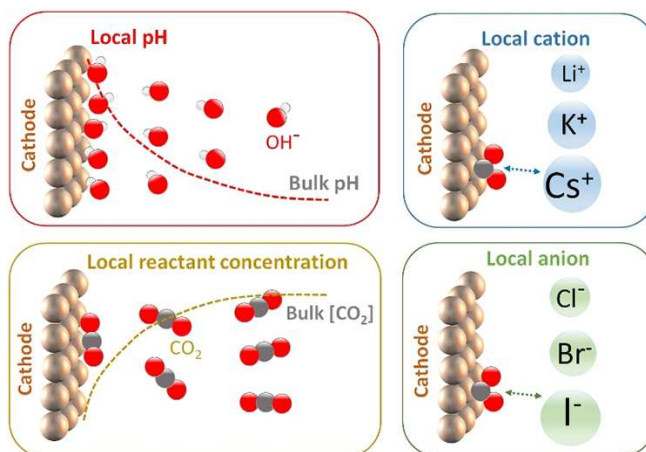
Accepted manuscript online: April 4, 2024

Version of record online: ■■■, ■■■

Aufsätze

CO₂ Utilization

M. Ma,* B. Seger* ————— e202401185

Rational Design of Local Reaction Environment for Electrocatalytic Conversion of CO₂ into Multicarbon Products

Beyond engineering the catalyst, rational design of the local reaction environment near the catalyst surface, including local pH, the choice of the species of cations and anions as well as local reactant/

intermediate concentrations, also acts as an effective approach for further improving the catalytic performance of CO₂ reduction to valuable multicarbon products.